frontiers | Frontiers in Earth Science

ORIGINAL RESEARCH
published: 14 April 2022
doi: 10.3389/feart.2022.862333

Sulfur and Oxygen Isotope Records of Sulfate-Driven Anaerobic Oxidation of Methane in Diffusion-Dominated Marine Sediments

Tingting Chen[1,2], Harald Strauss[3], Yunxin Fang[4], Zhiyong Lin[1,3,5], Xiaoming Sun[1,2,6]*, Jiarui Liu[7], Yang Lu[5], Xin Yang[1,2], Haixin Lin[1,2], Zhongwei Wu[1,2] and Xiao Lin[1,2]*

[1]School of Marine Sciences, Sun Yat-sen University, Guangzhou, China, [2]Guangdong Provincial Key Laboratory of Marine Resources and Coastal Engineering, Guangzhou, China, [3]Institut für Geologie und Paläontologie, Westfälische Wilhelms-Universität Münster, Münster, Germany, [4]Guangzhou Marine Geological Survey, Guangzhou, China, [5]Institut für Geologie, Centrum für Erdsystemforschung und Nachhaltigkeit, Universität Hamburg, Hamburg, Germany, [6]School of Earth Science and Engineering, Sun Yat-sen University, Guangzhou, China, [7]Department of Earth, Planetary and Space Sciences, University of California, Los Angeles, Los Angeles, CA, United States

OPEN ACCESS

Edited by:
Dong Feng,
Shanghai Ocean University, China

Reviewed by:
Xiaobin Cao,
Nanjing University, China
Xiting Liu,
Ocean University of China, China

***Correspondence:**
Zhiyong Lin
zhiyong.lin@uni-hamburg.de
Xiaoming Sun
eessxm@mail.sysu.edu.cn

Specialty section:
This article was submitted to Marine Geoscience, a section of the journal Frontiers in Earth Science

Received: *25 January 2022*
Accepted: *30 March 2022*
Published: *14 April 2022*

Citation:
Chen T, Strauss H, Fang Y, Lin Z, Sun X, Liu J, Lu Y, Yang X, Lin H, Wu Z and Lin X (2022) Sulfur and Oxygen Isotope Records of Sulfate-Driven Anaerobic Oxidation of Methane in Diffusion-Dominated Marine Sediments. Front. Earth Sci. 10:862333. doi: 10.3389/feart.2022.862333

Organoclastic sulfate reduction (OSR) and sulfate-driven anaerobic oxidation of methane (SD-AOM) are the two major microbial pathways for sulfate consumption in marine sulfur cycle. The relative changes of sulfur and oxygen isotope ratios in pore water sulfate are affected by the mode of microbial sulfate reduction and have been applied as an indicator for assessing methane excess environments. However, so far, this isotope proxy fails to distinguish sulfate reduction processes fueled by the oxidation of organic matter or by diffusing methane. To better understand the mechanism of sulfur and oxygen isotope partitioning during OSR and SD-AOM, coupled sulfur and oxygen isotopic compositions of pore water sulfate ($\delta^{34}S_{SO4}$ and $\delta^{18}O_{SO4}$) were investigated from four methane diffusing sites (CL56, CL57, CL59, and CL60) of the South China Sea, supplemented by carbon isotopic composition of dissolved inorganic carbon (DIC) and sulfur isotopic composition of pyrite in bulk sediments. Pore water sulfate and DIC concentrations, as well as calculated net sulfate reduction rates suggest that the sulfate reduction at site CL57 was mainly dominated by OSR, whereas sites CL56, CL59, and CL60 were likely impacted by both OSR and SD-AOM. Furthermore, the trend of cross-plotting $\delta^{18}O_{SO4}$ versus $\delta^{34}S_{SO4}$ values from site CL57 was distinguishable from sites CL56, CL59, and CL60, although all study sites show similar patterns to those derived from methane limited environments. This further indicates the trajectory of sulfur and oxygen isotope partitioning was affected by the mode of sulfate reduction (i.e., OSR vs. SD-AOM). At site CL57, the low net sulfate reduction rate would lead to enhanced oxidation of intermediate sulfur species during OSR, thus leading to a higher slope in the $\delta^{18}O_{SO4}$ vs. $\delta^{34}S_{SO4}$ cross-plot (1.26). In contrast, the higher net sulfate reduction rates at sites CL56, CL59, and CL60 due to the impact from SD-AOM would lead to lower slopes in the $\delta^{18}O_{SO4}$ vs. $\delta^{34}S_{SO4}$ cross-plots (0.78 ± 0.11). This study provides new insights into the sulfur and oxygen isotope systematics during microbial sulfate reduction processes in methane diffusing environments.

Keywords: organoclastic sulfate reduction, sulfate-driven anaerobic oxidation of methane, sulfur and oxygen isotopes in sulfate, methane diffusing environments, South China Sea

INTRODUCTION

As a bio-essential element, sulfur predominantly occurs as dissolved sulfate in the modern ocean (Canfield, 2001; Canfield et al., 2005). The formation of sulfide minerals, particularly pyrite (FeS_2), through microbial sulfate reduction processes and their preservation in sediments represent the key pathway for removing sulfate from the seawater in the global sulfur cycle (Jørgensen, 1982; Vairavamurthy et al., 1995). Organoclastic sulfate reduction (OSR) commonly occurs in organic-rich marine sediments, representing the dominant anaerobic metabolic pathway of organic matter remineralization (Jørgensen, 1982; Canfield, 2001). In addition, sulfate-driven anaerobic oxidation of methane (SD-AOM; e.g., Boetius et al., 2000; Orphan et al., 2001) is another key process for sulfate consumption and thus sulfide production, predominantly in methane-rich sediments along continental margins (Lin et al., 2016; Lin et al., 2017; Egger et al., 2018; Lin et al., 2018).

During microbial sulfate reduction (i.e., OSR and SD-AOM), multiple enzyme-catalyzed steps are involved (Rees, 1973; Brunner and Bernasconi, 2005; Eckert et al., 2011), and the mechanisms of the forward and backward enzymatic pathways affects the sulfate reduction rate (SRR; Böttcher et al., 1998; Aharon and Fu, 2000; Brunner et al., 2005). Many studies have documented that the sulfur isotope fractionation is affected by SRR during microbial sulfate reduction, i.e., the lower SRR, the larger sulfur isotope fractionation (Wortmann et al., 2001; Canfield et al., 2006). It was further identified that the combination of sulfur and oxygen isotopic compositions in the residual sulfate pool (i.e., $\delta^{34}S_{SO4}$ and $\delta^{18}O_{SO4}$) can reflect the SRR and decipher the mode of sulfate reduction in marine sediments (Böttcher et al., 1998; Böttcher et al., 1999; Aharon and Fu, 2000; Böttcher and Thamdrup, 2001; Aharon and Fu, 2003; Brunner et al., 2005; Wortmann et al., 2007; Farquhar et al., 2008; Turchyn et al., 2010; Brunner et al., 2012; Antler et al., 2013; Antler et al., 2014; Antler et al., 2015). This is mainly due to differing geochemical behavior of sulfur and oxygen isotope partitioning that occurs in each intracellular step during microbial sulfate reduction (Aharon and Fu, 2000; Brunner et al., 2005; Brunner et al., 2012; Antler et al., 2013).

Since isotopically lighter sulfur (^{32}S) is preferentially utilized during microbial sulfate reduction, the sulfur isotopic composition of residual sulfate ($\delta^{34}S_{SO4}$) increases with progressive sulfate reduction (Canfield, 2001), reflecting a combination of kinetic and equilibrium sulfur isotope fractionation through intracellular pathways (Wing and Halevy, 2014). In contrast, the behavior of oxygen isotopes of sulfate is affected by the exchange of oxygen atoms between the intermediate sulfur species formed during sulfate reduction and ambient water (Mizutani and Rafter, 1973; Fritz et al., 1989). Both, the oxygen and sulfur isotopic compositions of sulfate become gradually higher during microbial sulfate reduction and a constant $\delta^{18}O_{SO4}$ value will ultimately be obtained when an equilibrium of $\delta^{18}O_{SO4}$ with water ($\delta^{18}O_{H2O}$) is reached (Fritz et al., 1989; Brunner and Bernasconi, 2005; Wortmann et al., 2007). Generally, the slope in a cross-plot of $\delta^{18}O_{SO4}$ versus $\delta^{34}S_{SO4}$ (defined as 'SALP', e.g., Antler et al., 2013) prior to oxygen isotopes reaching apparent equilibrium is negatively correlated with the net SRR (Böttcher et al., 1998; Böttcher et al., 1999; Aharon and Fu, 2000; Brunner et al., 2005; Antler et al., 2013, 2015; Turchyn et al., 2016). A higher SALP is attributed to enhanced oxygen isotope exchange where more sulfite is re-oxidized to sulfate (Antler et al., 2013; Turchyn et al., 2016), while a lower SALP commonly results from higher net SRR (Antler et al., 2013).

Most of the reactive organic matter would be utilized via OSR in anoxic environments (e.g., Jørgensen, 1982). If reactive organic matter remains after dissolved sulfate has been depleted, its degradation would lead to methanogenesis (Martens and Berner, 1974; Froelich et al., 1979; Whiticar et al., 1986). Most of the methane generated from methanogenesis or release from methane hydrate deposits along continental margins would be consumed via SD-AOM within the sulfate-methane transition zone (SMTZ) in the sediment (Reeburgh, 1980; Hinrichs et al., 1999; Boetius et al., 2000; Regnier et al., 2011). Depending on the methane diffusing flux, the depths of the SMTZ can vary from several centimeters to tens or hundreds of meters below surface (Borowski et al., 1999; Egger et al., 2018).

Both, OSR and SD-AOM occur in sediments alone continental margins, but their SRR could vary significantly (Aharon and Fu, 2000; Böttcher et al., 2006; Antler et al., 2013; Gong et al., 2021). In methane-in-excess environments (e.g., cold seeps), methane is expelled from the sediment into the water column as gas bubbles (Valentine et al., 2001; Wallmann et al., 2006; Reeburgh, 2007, 2014). In these environments, the SALP values are low due to a typically high net SRR during SD-AOM (e.g., Antler et al., 2014; Antler et al., 2015; Feng et al., 2016; Gong et al., 2021). In contrast, when sulfate reduction is coupled with the oxidation of organic matter or diffusing methane, higher SALP values would be observed (Blake et al., 2006; Aller et al., 2010; Antler et al., 2013; Lin et al., 2017; Hu et al., 2020). However, no obvious differences in sulfur and oxygen partitioning during these two processes were identified. The relatively higher SALP values for both processes are likely caused by relatively slower net SRR in spite of the different electronic donors (Antler and Pellerin, 2018). Recently, the sulfur and oxygen isotopes of pore water sulfate have been explored to recognize the occurrence of SD-AOM in an active seep area (i.e., Haima seeps) of the South China Sea (Gong et al., 2021). The authors have observed small slopes of $\delta^{18}O_{SO4}$ vs. $\delta^{34}S_{SO4}$ (less than 0.5) in both methane-in-excess and diffusing environments and put forwarded that the $\delta^{18}O_{SO4}$ vs. $\delta^{34}S_{SO4}$ patterns in low methane flux environments are governed by variable isotope compositions of pore-water sulfate at greater depth. Since OSR and SD-AOM at depth (in methane diffusing

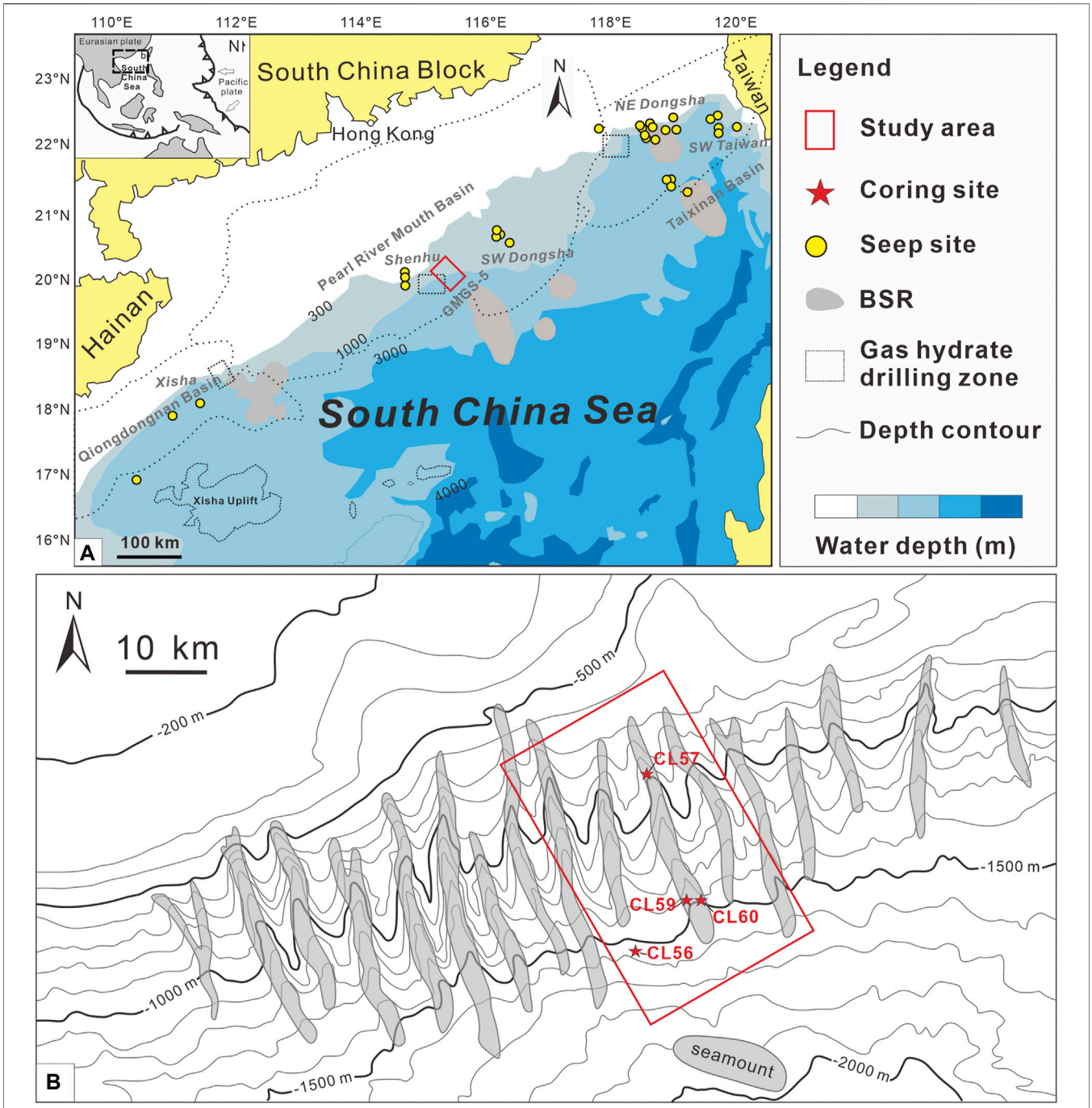

FIGURE 1 | Geological settings and locations of coring sites in the Shenhu area of the northern South China Sea. **(A)** The GMGS-5 gas hydrate drilling area is indicated by a red rectangle, which is located in the Pearl River Mouth Basin. **(B)** Locations of the four coring sites are marked by red stars (after Sun et al., 2012; Lin et al., 2017).

environments) represent the most common processes for sulfate reduction in modern marine sediments, knowledge about the mechanisms and environmental controls on the associated isotope evolution is essential for us to better constrain the oceanic sulfur cycling.

In order to explore the isotope partitioning during OSR and SD-AOM, sulfur and oxygen isotopic compositions of dissolved sulfate were investigated in this study from multiple sites in the Shenhu area, a typical methane diffusing area in the South China Sea (Yang et al., 2010; Wu L. et al., 2013; Wei et al., 2019). Concentrations of pore water sulfate and dissolved inorganic carbon (DIC) and the carbon isotopic composition ($\delta^{13}C_{DIC}$) were supplemented to constrain the principal sulfate reduction process at the study sites.

GEOLOGICAL BACKGROUND

As one of the largest marginal seas in the western Pacific Ocean, the South China Sea is surrounded by the Eurasian Plate, the Pacific Plate and the Indo-Australian Plate (Suess, 2005). The northern slope of the South China Sea is characterized by a typical passive continental margin. Seep carbonates and gas hydrates were widely discovered in this location (Zhang H. Q. et al., 2007; Han et al., 2008; Tong et al., 2013; Feng and Chen, 2015; Liang et al., 2017). The occurrence of gas hydrate was confirmed for several target areas, including the Shenhu area (Zhang H. T. et al., 2007; Yang et al., 2008; Wu D. D. et al., 2013; Wang et al., 2014), the Dongsha area (Han et al., 2008; Feng and Chen, 2015), the Xisha Through (Jiang et al., 2008), as well as the Qiongdongnan Basin (Liang et al., 2017; Wei et al., 2019; Ye et al., 2019). The Shenhu area is located in the middle of the northern slope of the South China Sea. Tectonically, it is located within the Pearl River Mouth Basin (Wu D. et al., 2011), which is characterized by organic-rich sediment ranging in thickness from 1000 to 7000 m (Li et al., 2010; Wu N. et al., 2011). Bottom-simulating reflectors (BSRs), as an indicator for bottom the gas hydrate stabilization zone, are widely identified in the Shenhu area (Yu et al., 2014; Yang et al., 2017; Zhang et al., 2019). Furthermore, high-angle fractures and diapir structures are highly developed in this area, which is essential for methane-bearing fluid migration and gas hydrate formation (Wu et al., 2009).

SAMPLES AND METHODS

Samples

In 2018, GMGS-5 drilling expedition was conducted by the Guangzhou Marine Geological Survey in the northwestern part of the South China Sea (Wei et al., 2019). Studied sediment samples were obtained from four gravity cores collected during the GMGS-5 Cruise in the Shenhu area (**Figure 1**). The water depths of these sites vary from 990 to 1534 m. The sediments show homogeneous lithologies at all sites, mainly consisting of green-gray clay and silt. The pore water samples were extracted at 20 cm intervals using Rhizon samplers with a membrane pore size of 0.2 μm (Seeberg-Elverfeldt et al., 2005). About 10–20 ml pore water sample was extracted from each depth interval and stored at 4°C until further analysis.

Analytical Methods

The concentrations of dissolved sulfate (SO_4^{2-}), calcium (Ca^{2+}), and magnesium (Mg^{2+}) were measured at the Instrumental Analysis and Research Center, Sun Yat-sen University. An Ion Pac AS14-type column and an Ion Pac AS12A-type column were used for anion and cation separation, respectively. Pore water samples were diluted 500-fold with deionized water. A mixed solution with Na_2CO_3 (3.5 mM) and $NaHCO_3$ (1.0 mM) was used as eluent (1.0 ml/min) for sulfate concentration analysis using a Dionex ICS-5000 ion chromatograph. Meanwhile, an 18 mM methanesulfonic acid solution was used as eluent (1.0 ml/min) for Ca^{2+} and Mg^{2+} concentrations using a Dionex ICS-900 ion chromatograph.

For DIC concentration and $\delta^{13}C_{DIC}$ analyses, 0.2 ml of each pore water sample was injected into an evacuated septum tube containing concentrated phosphoric acid. The liberated CO_2 gas was separated by a gas chromatographic column in 75°C and then transferred to a continuous flow isotope ratio mass spectrometer (ThermoFisher MAT253 mass spectrometer interfaced with a Finnigan GasBench) for isotope ratio measurements. Isotope results are reported in the delta notation as per mil difference from the Vienna Peedee Belemnite (V-PDB) standard. The analytical precision was better than ±0.2‰ for $\delta^{13}C_{DIC}$ values. A 50 mM Na_2CO_3 + $NaHCO_3$ standard solution was diluted into concentrations of 0.49, 2.67, 5.83, 9.57, 24.54, and 34.71 mM to determine the calibrations curves. The linear correlation between the intensity of released CO_2 gas and the DIC concentrations of Na_2CO_3 + $NaHCO_3$ standard solution was used for calculating the DIC concentration in the samples. Analyses were conducted at the Third Institute of Oceanography, Ministry of Natural Resources.

For sulfate sulfur and oxygen isotope analyses, pore water samples were filtered (<0.45 μm) and sulfate was precipitated as $BaSO_4$ using an 8.5 wt% $BaCl_2$ solution at pH 2 and sub-boiling conditions. The $BaSO_4$ precipitates were washed with deionized water and filtered through a pre-weighed 0.45 μm cellulose nitrate membrane filter. Precipitates were dried at 40°C and weighed out to calculate the yields. For $\delta^{34}S_{SO4}$ analysis, about 200 μg of $BaSO_4$ precipitate mixed with an equal amount of vanadium pentaoxide (V_2O_5) were combusted to SO_2, and subsequently transferred to a ThermoScientific Delta V Advantage mass spectrometer interfaced to a Flash EA IsoLink CN elemental analyzer (EA-IRMS). The measurements were carried out at the Institut für Geologie und Paläontologie, Westfälische Wilhelms-Universität Münster. The sulfur isotope values are reported in per mil relative to the Vienna Canyon Diablo Troilite (V-CDT) standard and the analytical precision is better than ±0.3‰:

$$\delta^{34}S\ (‰,\ V-CDT) = \left[\left(\frac{\left({}^{34}S/{}^{32}S\right)_{sample}}{\left({}^{34}S/{}^{32}S\right)_{V-CDT}}\right)-1\right]\times 1000$$

The analytical performance was calibrated by international reference materials IAEA-S1 ($\delta^{34}S$ = −0.30‰), IAEA-S2 ($\delta^{34}S$ = +21.55‰), IAEA-S3 ($\delta^{34}S$ = −31.4‰) and NBS 127 ($\delta^{34}S$ = +21‰).

Oxygen isotopic compositions of $BaSO_4$ precipitates were determined following combustion at 1450°C in a pyrolysis unit (ThermoFinnigan TC/EA) coupled to a ThermoScientific Delta V Plus mass spectrometer at the Institut für Geologie und Paläontologie, Westfälische Wilhelms-Universität Münster. Results are reported as $\delta^{18}O_{SO4}$ relative to the Vienna Standard Mean Ocean Water (V-SMOW) with an analytical precision better than ±0.5‰:

$$\delta^{18}O\ (‰,\ V-SMOW) = \left[\left(\frac{\left({}^{18}O/{}^{16}O\right)_{sample}}{\left({}^{18}O/{}^{16}O\right)_{V-SMOW}}\right)-1\right]\times 1000$$

Measurements of the $\delta^{18}O_{SO4}$ were calibrated with international reference materials NBS 127 ($\delta^{18}O$ = 8.59‰), IAEA-S0-5 ($\delta^{18}O$ = 12.13‰), and IAEA-S0-6 ($\delta^{18}O$ = −11.35‰).

For total organic carbon (TOC) content measurements, about 2 g bulk sediment powder was pre-acidified by 1 M HCl for 6 h to remove inorganic carbon. The residue was washed thoroughly with deionized water for three times and dried at 60°C before analysis. TOC contents were analyzed using an elemental analyzer (Flash 2000 CHNS/O, Thermo Fisher) at the Third Institute of Oceanography, Ministry of Natural Resources. The results were calibrated with reference material BBOT (C = 72.53 wt%) and the analytical reproducibility was better than 3%.

The chromium reduction technique was applied to extract solid-phase sulfur from sediment samples (Canfield et al., 1986; Rice et al., 1993). About 3 g bulk sediment powder was reacted with 20 ml 8 M HCl for 1 h in an O_2-free round bottom flask with continuous N_2 flow for extracting acid volatile sulfide (AVS, mainly iron monosulfides). However, no AVS was observed in all samples. Subsequently, the residue was reacted with 30 ml chromous (II) chloride solution (1 M) at near-boiling temperatures for 2 h to extract chromium reducible sulfur (CRS, mainly pyrite). The liberated hydrogen sulfide gas was trapped as zinc sulfide precipitate in 4% zinc acetate-acetic acid solution. Zinc sulfide was converted into silver sulfide (Ag_2S) by adding 10 ml of 0.1 M silver nitrate solution. The Ag_2S precipitates were collected by membrane filtration (<0.45 μm) and dried at 40°C. The CRS contents were determined gravimetrically based on the dried Ag_2S yields. For sulfur isotope analysis, 200 μg Ag_2S mixed with an equal amount of vanadium pentaoxide (V_2O_5) were combusted to SO_2 using a Thermo Scientific Delta V Advantage mass spectrometer linked to a Flash EA IsoLink CN Elemental Analyzer (EA-IRMS) at the Institut für Geologie und Paläontologie, Westfälische Wilhelms-Universität Münster. The $\delta^{34}S_{CRS}$ values are reported relative to the Vienna Canyon Diablo Troilite (V-CDT) with an analytical precision better than ±0.3‰. The analytical performance was monitored with international reference materials IAEA-S1 ($\delta^{34}S$ = −0.30‰), IAEA-S2 ($\delta^{34}S$ = +21.55‰), IAEA-S3 ($\delta^{34}S$ = −31.4‰), and NBS 127 ($\delta^{34}S$ = +21‰).

Calculation of the Diffusive Sulfate Flux

The linear depth profiles of sulfate concentration at all study sites indicate that sulfate consumption was mainly dominated by SD-AOM (Berner, 1980; Borowski et al., 1996). In this case, the upward flux of methane can be determined via the downward sulfate flux assuming that sulfate flux is stoichiometrically balanced by the methane flux due to SD-AOM (Borowski et al., 1996; Niewöhner et al., 1998) and that sulfate flux consumed by OSR is insignificant.

The vertical sulfate diffusive flux J (nmol cm^{-2} d^{-1}) can be calculated according to Fick's First Law under steady-state conditions (Schulz, 2006):

$$J = -\varphi \cdot D_s \cdot \partial C/\partial z \quad (1)$$

where φ is the sediment porosity, D_s is the diffusion coefficient for bulk sediments, C is the concentration of sulfate, z is the depth below the seafloor, and $\partial C/\partial z$ is the linear gradient of sulfate concentrations. The porosities of these sites were set at 0.7 for CL56 and CL60, 0.68 for CL59, and 0.66 for CL57, according to the measured porosities from a nearby site (Wu L. et al., 2013). To compensate for tortuosity, the whole sediment diffusion coefficient (D_s) was calculated by the empirical equation (Iversen and Jørgensen, 1993): $D_s = D_0/(1 + 3\ (1 - \varphi))$, using the molecular diffusion coefficient in seawater (D_0) and calculated sediment porosity (φ). Seawater D_0 of sulfate is 4.94 × 10^{-1} cm^2 d^{-1}at a mean temperature of 5°C (Schulz, 2006).

Modeling of Net Sulfate Reduction Rates

A steady-state scenario at the study sites is supported by the linear relationship of sulfate concentration depth profiles. Therefore, one-dimensional reaction-transport modeling of pore water sulfate concentration profiles can be developed to estimate the net rates of sulfate reduction in subsurface sediments using the software PROFILE (Berg et al., 1998). This numerical procedure assumed that sulfate transport only occurs *via* molecular diffusion. This assumption is largely consistent with the study sites from Shenhu area where subsurface sediments are dominantly affected by sulfate and methane diffusion instead of advection as usually seen at methane seeps (Hu et al., 2020). Since bioirrigation and bioturbation only occur in the uppermost sediments (Van Cappellen and Wang, 1996), data from shallow sediments were not considered in our model. Here, pore water sulfate concentration at the top and sulfate flux at the bottom of the calculation domain were chosen as boundary conditions. The PROFILE model divided the sediment column into several discrete depth intervals (e.g., 3 zones). A constant rate of production or consumption as a function of depth was gained via the best curve fitting of measured concentration profiles (Berg et al., 1998). As these gravity cores only penetrated part of the sulfate zone, the concentration gradients of sulfate used in the modeling were extrapolated *via* the most linear part of the sulfate depth profiles and directed into the SMTZ where sulfate concentrations reach zero. The modeled volumetric rates are in units of nmol cm^{-3} d^{-1}, and the depth-integrated rates are presented in units of nmol cm^{-2} d^{-1}.

RESULTS

Concentrations of Dissolved Sulfate, Calcium, Magnesium, Inorganic Carbon, and $\delta^{13}C_{DIC}$ Values

The concentrations of dissolved SO_4^{2-}, Ca^{2+}, and Mg^{2+} in pore water are presented in **Figures 2A–C**. Overall, sulfate concentrations remain constant at the uppermost 100 cmbsf, followed by a linear decrease to the bottom of the cores. At sites CL56, CL59, and CL60, the sulfate concentrations decline rapidly from near seawater values to ~10 mM with similar gradients. In contrast, the decrease of sulfate concentration at site CL57 is slower, with a value of 24.3 mM at the bottom. Similarly, the Ca^{2+} concentrations display downward decreasing trends at sites CL56, CL59, and CL60, dropping from 8.9 to 5.4 mM, 8.6–5.0 mM, and 8.7–4.6 mM, respectively. The decrease in Ca^{2+} concentration at site CL57 is less pronounced, changing from 9.0 to 7.1 mM. The

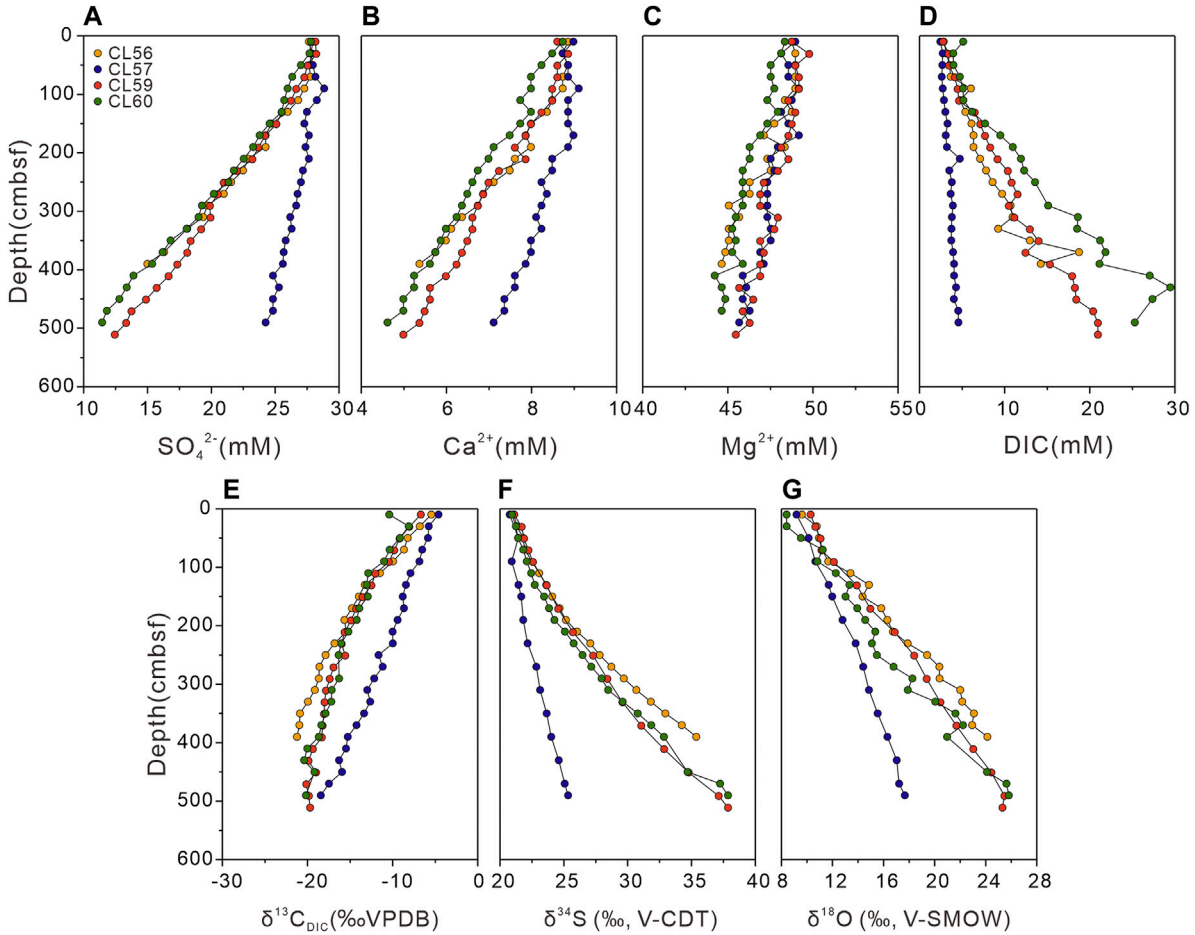

FIGURE 2 | Depth profiles of pore water geochemical data for the study sites. **(A)** sulfate (SO_4^{2-}) concentration; **(B)** calcium (Ca^{2+}) concentration; **(C)** magnesium (Mg^{2+}) concentration; **(D)** dissolved inorganic carbon (DIC) concentration; **(E)** carbon isotopic composition of DIC ($\delta^{13}C_{DIC}$) in per mil (‰) relative to the Vienna Peedee Belemnite Standard (V-PDB); **(F)** sulfur isotopic composition of sulfate ($\delta^{34}S_{SO4}$) in per mil (‰) relative to the Vienna Canyon Diablo Troilite standard (V-CDT); **(G)** oxygen isotopic composition of sulfate ($\delta^{18}O_{SO4}$) in per mil (‰) relative to the Vienna Standard Mean Ocean Water standard (V-SMOW). cmbsf-centimeters below seafloor.

Mg^{2+} concentrations are decreasing slowly from top to depth without any obvious difference at these sites.

The DIC concentrations reveal increasing trends with depth at the study sites with different gradients (**Figure 2D**). In particular, the DIC concentrations of site CL57 show a narrow range from 2.5 to 4.6 mM. For sites CL56, CL59, and CL60, the DIC concentrations vary from 2.8 to 18.7 Mm, 2.8–21.0 mM, 4.0–29.5 mM, respectively. The $\delta^{13}C_{DIC}$ values exhibit decreasing trends with depth (**Figure 2E**), ranging from −5.4 to −21.2‰ at site CL56, −4.6 to −18.4‰ at site CL57, −6.7 to −20.1‰ at site CL59, and −8.1 to −20.4‰ at site CL60, respectively.

Sulfur and Oxygen Isotopic Compositions of Sulfate

The sulfur and oxygen isotopic compositions of pore water sulfate from the study sites are shown in **Figures 2F,G**. Both, $\delta^{34}S_{SO4}$ and $\delta^{18}O_{SO4}$ values increase linearly with depth. For sites CL56, CL59, and CL60, the $\delta^{34}S_{SO4}$ values display relatively rapid increases compared to site CL57, ranging from 21.1 to 35.4‰, 21.1–37.9‰, and 20.9–37.9‰ respectively. In contrast, $\delta^{34}S_{SO4}$ values vary from 20.8 to 25.3‰ at site CL57. Similarly, the $\delta^{18}O_{SO4}$ values at sites CL56, CL59, CL60, and CL57 increase from 9.6 to 24.1‰, 10.3–25.5‰, 8.4–25.8‰, and from 9.2 to 17.7‰, respectively.

Contents of Total Organic Carbon, Total Sulfur, Chromium Reducible Sulfur, and $\delta^{34}S_{CRS}$ Values of Bulk Sediments

TOC contents for bulk sediments and their depth trends (**Figure 3A**) are nearly identical (0.77–1.04 wt%) among study sites for the first 100 cmbsf., the depth trends for sites CL56, CL59, and CL60 are similar, increasing from 0.86 to 1.48 wt%, 0.79 to 1.58 wt%, and 0.86 to 1.57 wt%. For site CL57, however, the TOC contents exhibit an inverse trend, decreasing from 1.21 to 0.54 wt%. Sulfur contents of sediments for sites CL56, CL57, and CL60 are ranging from 0.15 to 0.80 wt%, 0.14 to 0.45 wt%, and 0.15 to 0.78 wt%, respectively.

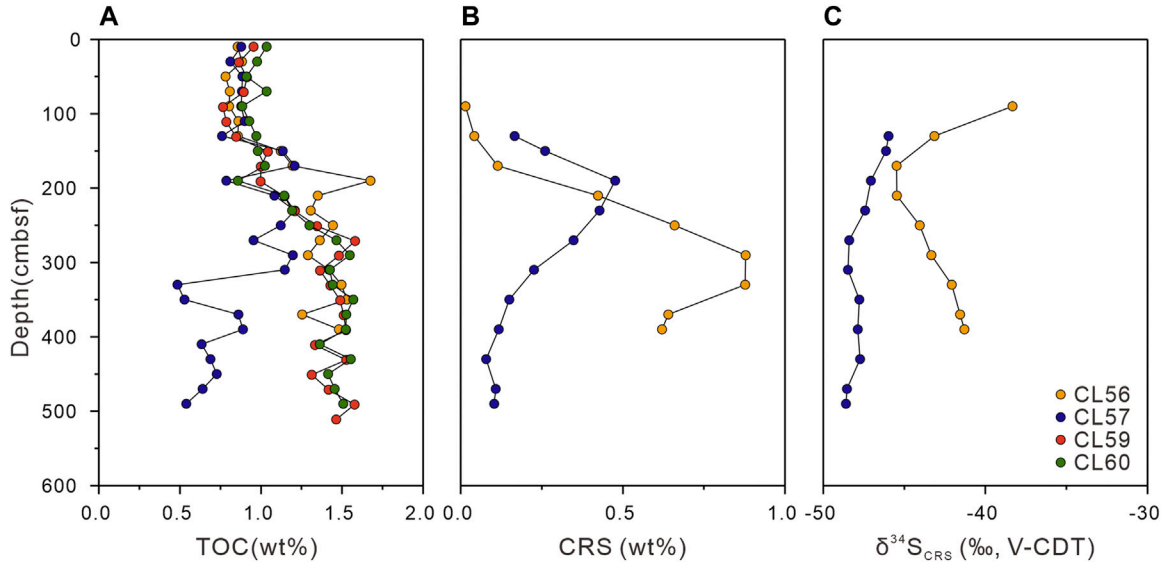

FIGURE 3 | Depth profiles of geochemical data of sediments for the study sites: **(A)** total organic carbon (TOC) contents; **(B)** chromium reducible sulfur (CRS) contents; **(C)** stable sulfur isotopic compositions of CRS ($\delta^{34}S_{CRS}$).

Notably, TOC/TS (C/S ratios) vary from 1.6 to 5.6 for sites CL56, 1.9 to 6.4 for CL57 and 1.9 to 6.2 for CL60, and show disparate patterns among these sites below ~200 cmbsf, with increasing trends for site CL57 and decreasing trends to the bottom cores for sites CL56 and CL60 (**Supplementary Table S2**).

The CRS content for bulk sediments from sites CL56 and CL57 were analyzed (**Figure 3B**). At shallow depths for both sites, the CRS contents are below detection limit. At site CL56, the CRS contents reveal an increase from 0.01 to 0.88 wt% with a peak at 290 cmbsf, followed by a decrease to 0.62 wt% at the bottom of the core. At site CL57, the CRS contents slightly increase from 0.17 to 0.48 wt%, and subsequently decrease from 0.48 to 0.10 wt%, with a peak at 190 cmbsf. The $\delta^{34}S_{CRS}$ values range from −45.5 to −38.3‰ and −48.6 to −46.0‰ at sites CL56 and CL57, respectively (**Figure 3C**). From 90 cmbsf to 170 cmbsf at site CL56, the $\delta^{34}S_{CRS}$ values show a decreasing trend ranging from −38.3 to −45.5‰. Further down, $\delta^{34}S_{CRS}$ values increase from −45.5 to −41.3‰ at the bottom of the core. In contrast, the $\delta^{34}S_{CRS}$ values at site CL57 reveal a slightly decreasing tread with depth from −46.0 to −48.6‰.

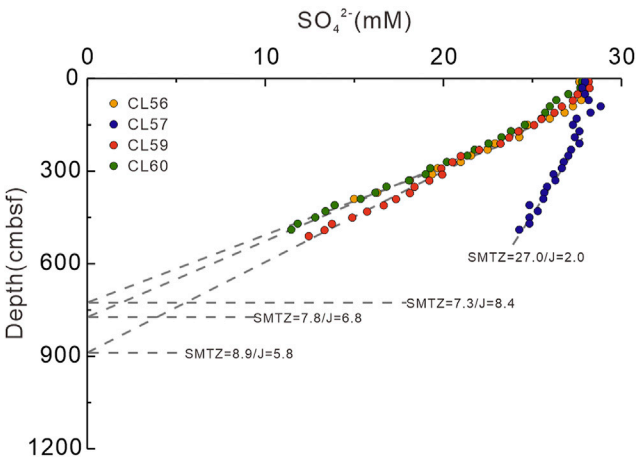

FIGURE 4 | Sulfate diffusive fluxes (J, nmol cm^{-2} d^{-1}) and corresponding depths of SMTZ (m) for the study sites via linear regression fits of sulfate concentration profiles. A higher flux corresponds to a relatively shallower depth of SMTZ. The calculated sulfate flux is roughly equivalent to the methane flux diffusing from below at each site.

Calculated Sulfate Fluxes and Rates of Sulfate Reduction

The estimated fluxes by linear regression of sulfate concentrations for sites CL56, CL57, CL59, and CL60 are 30.8, 7.1, 21.1, and 24.8 mmol m^{-2} a^{-1}, respectively. According to the corresponding sulfate gradients, the depths of the SMTZ where sulfate concentrations decline to zero are shown in **Figure 4**. The estimated SMTZs for sites CL56, CL57, CL59, and CL60 are located at 7.3, 27.0, 8.9, and 7.8 mbsf, respectively.

The net rates of sulfate reduction calculated by the PROFILE model are shown in **Figure 5**. The model divided the sediment column into several zones with different reaction rates, and the depth-integrated rates of sulfate reduction (i.e., the overall rates of sulfate consumption across the whole calculation domains) for sites CL56, CL57, CL59, and CL60 are 8.0, 0.7, 6.3, and 7.5 nmol cm^{-2} d^{-1}. Specifically, for sites CL56, CL59, and CL60, a distinct peak of volumetric sulfate reduction rate (i.e., rate of sulfate consumption for each discrete sediment column) can be seen near the SMTZ, while no net sulfate consumption is found above the SMTZ. However, at site CL57, a relatively lower peak of volumetric sulfate reduction

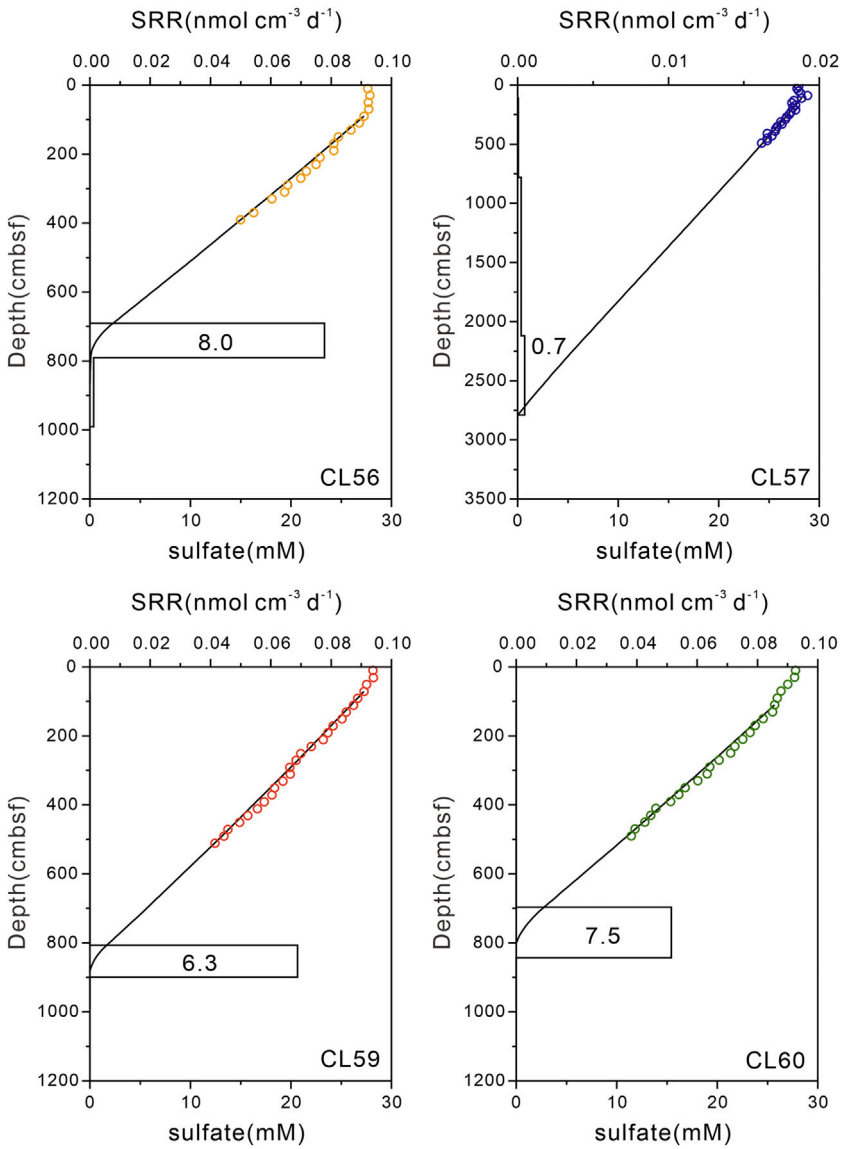

FIGURE 5 | Best fitted sulfate concentration profiles and modeled net sulfate reduction rates (nmol cm^{-3} d^{-1}) for study sites. Sulfate concentrations in the upper tens of centimeters remain more or less invariant due to bioirrigation and thus are not considered in the model. The depth-integrated rate of sulfate reduction for each core are noted in the box.

rate can be identified, and the net sulfate consumption is low throughout the entire core.

DISCUSSION

Sulfate Reduction in the Pore Water and Evidences for Organoclastic Sulfate Reduction and Sulfate-Driven Anaerobic Oxidation of Methane

The sulfate consumption in marine sediments is mainly controlled by **(1)** organoclastic sulfate reduction (OSR, Berner, 1980) and 2) sulfate-driven anaerobic oxidation of methane (SD-AOM, Hinrichs et al., 1999; Boetius et al., 2000). Steep sulfate gradients from seafloor to the SMTZ normally indicate high methane flux in the sediments (Borowski et al., 2000; Hoehler et al., 2000; Dickens, 2001). Sulfate reduction in the sediments affect the shape of pore water sulfate profiles (Niewöhner et al., 1998; Dickens, 2001; Hensen et al., 2003). It was proposed that a linear depletion of sulfate normally reflects co-consumption of sulfate and methane mainly by SD-AOM under steady-state conditions (Jørgensen and Kasten, 2006). In contrast, concave up and down types generally result from OSR-dominated consumption or changes in the methane flux from below under non-steady state conditions (Hensen et al., 2003;

Jørgensen and Kasten, 2006). However, it was found that the co-occurrence of OSR and SD-AOM in the sediment can also lead to a nearly linear sulfate profile (Malinverno and Pohlman, 2011).

In the uppermost sediments at the study sites (above 100 cmbsf), the sulfate concentrations remain nearly constant. Likely, this reflects sufficient replenishment of sulfate from the overlying seawater or sulfide reoxidation caused by near surface bioturbation or bioirrigation (Fossing et al., 2000; Treude et al., 2005; Claypool et al., 2006; Coffin et al., 2008; Minami et al., 2012), which is common in near-surface sediments in the northern slope of the South China Sea (Yang et al., 2010; Ye et al., 2016). Below 100 cmbsf, sulfate concentration profiles of all sites reveal linear depletion. The non-zero sulfate concentrations at the bottom of the cores suggest that the gravity cores have not penetrated the SMTZ. The depths of the SMTZ are obtained by linear regression (**Figure 4**). Previous studies suggested that the depth of the SMTZ is generally related to the upward methane flux, where a shallower depth of the SMTZ is corresponding to a higher methane flux (Borowski et al., 1996; Dickens, 2001). Assuming the methane flux is identical to the sulfate flux, it is apparent that the methane flux at site CL57 (2.0 nmol cm^{-2} d^{-1}) is much lower than for sites CL56, CL59, and CL60 (5.8–8.4 nmol cm^{-2} d^{-1}). Two groups can be divided according to the distinct depths of the SMTZs and the methane fluxes: 1) sites CL56, CL59, and CL60 with shallower depths of the SMTZ as "group A", and 2) site CL57 with a greater depth of the SMTZ as "group B".

The methane fluxes obtained in this study are much lower compared to those seep sites characterized by gas bubble ebullition and remarkably shallower SMTZs (several centimeters; Aharon and Fu, 2000; Luff and Wallmann, 2003). Our results are similar to previous studies in the Shenhu area (Wu L. et al., 2013; Hu et al., 2020), which clearly indicates a typical methane diffusing environment in the study areas. Recently, OSR was identified as a significant microbial pathway responsible for the consumption of pore water sulfate across the SMTZ (Komada et al., 2016; Egger et al., 2018; Jørgensen et al., 2019). In addition, it was argued that it is inappropriate to propose SD-AOM as the dominant sulfate reduction process only based on a linear sulfate gradient (Malinverno and Pohlman, 2011; Jørgensen et al., 2019). Consequently, discriminating the microbial pathways fueling sulfate reduction (i.e., OSR and SD-AOM) in the sediments becomes critical for us to better understand the sedimentary sulfur cycling.

The concentration and the carbon isotopic composition of DIC in sediments have been used to interpret the mode of sulfate reduction (Kastner et al., 2008; Chatterjee et al., 2011; Luo et al., 2013). In alkaline environments, DIC is predominantly composed of bicarbonate (HCO_3^-) (Ussler and Paull, 2008). According to the equations for OSR and SD-AOM, OSR produces two mol of bicarbonate by consuming one mol sulfate ($2CH_2O + SO_4^{2-} \rightarrow 2HCO_3^- + H_2S$), while SD-AOM process produces one mol of bicarbonate by utilizing one mol sulfate ($CH_4 + SO_4^{2-} \rightarrow HCO_3^- + HS^- + H_2O$; Kastner et al., 2008). Thus, the ratios of the production of DIC (ΔDIC) to the consumption of sulfate (ΔSO_4^{2-}) was applied to differentiate the relative contribution of OSR (ΔDIC: ΔSO_4^{2-} = 2:1) and SD-AOM

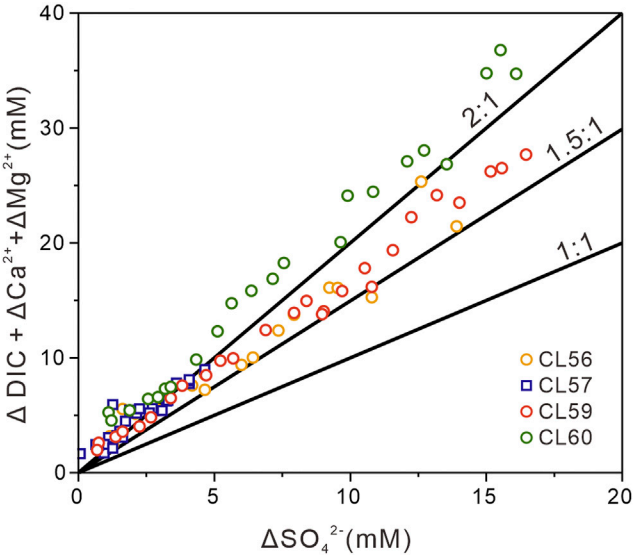

FIGURE 6 | Plots of sulfate removed versus DIC elevated corrected for calcium and magnesium loss due to authigenic carbonate precipitation. The ΔDIC, ΔCa^{2+}, and ΔSO_4^{2-} are the differences between seawater values (2.1 mM for DIC, 10.3 mM for Ca^{2+}, and 28.9 mM for ΔSO_4^{2-}; Chen et al., 2010) and measured results in this study. The ΔMg^{2+} represents the loss of magnesium with depth relative to the uppermost pore water (~49 mM). The diagonal lines indicate 2:1, 1.5:1, and 1:1 ratio. The 2:1 ratio is consistent with sulfate reduction processes dominated by OSR, while the 1:1 ratio is consistent with sulfate reduction fueled by anaerobic oxidation of methane (i.e., SD-AOM).

(ΔDIC: ΔSO_4^{2-} = 1:1) (Masuzawa et al., 1992). Since the precipitation of carbonate in a high alkalinity environment can lead to the consumption of dissolved Ca^{2+} and Mg^{2+} (Rodriguez et al., 2000), the combination of $\Delta DIC+\Delta Ca^{2+}+\Delta Mg^{2+}$ can be used to reflect the accurate DIC concentrations (**Figure 6**). Here, ΔDIC, ΔCa^{2+}, and ΔSO_4^{2-} are calculated relative to the typical seawater values for DIC (2.1 mM), Ca^{2+} (10.3 mM), and SO_4^{2-} (28.9 mM) (Chen et al., 2010). As the measured Mg^{2+} concentrations at the uppermost depths from all sites are lower than the typical seawater value (53.2 mM, Chen et al., 2010), ΔMg^{2+} is calculated relative to the highest concentration at the top of the study sites (49.0 mM). Data from sites CL56 and CL59 falls into the area between the slopes of 2:1 and 1:1, suggesting the co-occurrence of OSR and SD-AOM at these sites. In contrast, data from site CL57 mainly cluster at or near the slope of 2:1, which indicates that OSR is the predominant process at these sites. Although the data from site CL60 also cluster near the slope of 2:1, we suggest a contribution of SD-AOM cannot be completely ruled out, since the pore water sulfate pattern of site CL60 is similar to sites CL56 and CL59.

Pore water DIC is mainly derived from: 1) seawater ($\delta^{13}C_{SW}$: ~ 0‰, Claypool et al., 2006), 2) OSR ($\delta^{13}C_{OM}$: −20‰, Chen et al., 2012), and 3) SD-AOM ($\delta^{13}C_{CH4}$: −35‰ ~ −80‰, Masuzawa et al., 1992). Consequently, the $\delta^{13}C_{DIC}$ values are often applied to indicate the sources of DIC (Borowski et al., 2000; Sivan et al., 2007; Chen et al., 2010; Malinverno and Pohlman, 2011; Hu et al.,

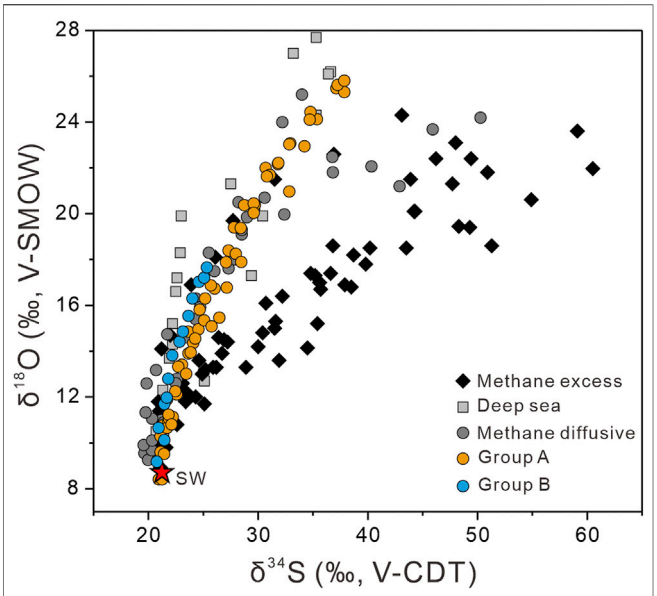

FIGURE 7 | Plots of $\delta^{18}O_{SO4}$ versus $\delta^{34}S_{SO4}$ of study sites (group A: CL56, CL59, and CL60; group B: CL57) departures from the initial sulfate values ($\delta^{34}S$ = +20.24‰, Tostevin et al., 2014; $\delta^{18}O$ = +8.7‰, Johnston et al., 2014), comparing with compiled data from methane excess, methane diffusive, and deep-sea sediments (Aharon and Fu, 2000; Blake et al., 2006; Böttcher et al., 2006; Aller et al., 2010; Strauss et al., 2012; Antler et al., 2014; Antler et al., 2015; Lin et al., 2017; Hu et al., 2020).

2015). The $\delta^{13}C_{DIC}$ values for CL57 are between the seawater value (~0‰) and typical organic matter value (−20‰), suggesting a mixture of DIC derived from diffusing seawater, OSR and potential SD-AOM. This agrees with the 2:1 slope of ($\Delta DIC+\Delta Ca^{2+}+Mg^{2+}$): ΔSO_4^{2-}. The decrease in $\delta^{13}C_{DIC}$ with depth implies an increasing contribution from OSR. In contrast, the $\delta^{13}C_{DIC}$ values at the bottom of the cores for sites CL56, CL59 and CL60 are slightly lower than −20‰, suggesting more contributions from SD-AOM. The lower C/S ratios of bulk sediments corresponding to considerable addition of CRS also indicate more intense SD-AOM at site CL56 relative to that at site CL57 (**Supplementary Table S2**; Liu et al., 2020; Liu et al., 2021; Miao et al., 2021).

Coupled Sulfur and Oxygen Isotopic Compositions of Dissolved Sulfate: Constraints on Sulfate Reduction

Overall, cross-plots of $\delta^{18}O_{SO4}$ versus $\delta^{34}S_{SO4}$ values (**Figure 7**) exhibit a linear increase with depth from seawater values ($\delta^{34}S$ = +21.24‰, Tostevin et al., 2014; $\delta^{18}O$ = +8.7‰, Johnston et al., 2014). Moreover, all the data for this study resemble isotope patterns derived from the methane diffusive environments (**Figure 7**; Antler et al., 2015). Interestingly, the SALP at each site exhibits two different trends (**Figure 8**). For the upper sediment column (~200 cmbsf), $\delta^{18}O_{SO4}$ increases more rapidly than $\delta^{34}S_{SO4}$, resulting in rather higher SALP (1.49–2.82). Such relatively higher SALP values in shallow sediments have also been observed elsewhere (Antler et al., 2013; Antler et al., 2015; Lin et al., 2017). This SALP pattern is consistent with the relatively constant sulfate concentrations (**Figure 2A**) and higher sulfur isotopic compositions (**Figure 3C**) in the upper sediment column, which was explained by the enhanced sulfur disproportionation or reoxidation of sulfide to sulfate (Böttcher et al., 1999; Böttcher and Thamdrup, 2001; Böttcher et al., 2006; Lin et al., 2017). Likely, bioturbation or bioirrigation processes the shallow sediments canfacilitate the penetration of oxygen and thus enhance the oxidative sulfur cycle (Minami et al., 2012).

At greater depth, the SALP value becomes lower at each site, suggesting that the oxidation of intermediate sulfur species is less significant. The range of SALP values (from 0.74 to 1.26) is similar to other environments where methane was undetectable and sulfate reduction is fueled by organic matter oxidation (Antler et al., 2013; Hu et al., 2020). Still, a difference in the SALP can be identified between site CL57 and the others (sites CL56, CL59, and CL60), with the SALP from site CL57 showing a higher value (1.26, see **Figure 9**). This high SALP value indicates a slower net SRR at this site, which could result from a low supply of the electron donor (i.e., organic matter) (**Figure 3A**). In addition, this pattern agrees with the low content and the strongly negative sulfur isotopic composition of CRS at this site (**Figures 3B,C**). In contrast, the sulfate and DIC concentration profiles from sites CL56, CL59 and CL60 indicate that SD-AOM plays a key role in sulfate consumption at depth. Aharon and Fu (2000) proposed that the sulfate reduction rate is a function of the type of organic carbon substrate (e.g., methane and organic matter), which can affect the SALP. It has been suggested that a change in the principal electron donor from organic matter to methane can lead to less reoxidation of the intermediate sulfur species, which may result in a lower SALP (Antler et al., 2014; Yoshinaga et al., 2014). This provides an alternative cause for explaining the lower SALP values at these sites.

To calculate the net sulfate reduction rate for each site, one-dimensional transport-reaction modeling was applied in this study using the PROFILE model (Berg et al., 1998). The depth-integrated rates calculated by the model were considered to represent the net rates of sulfate reduction across each site. The net sulfate reduction rates are much higher for sites CL56, CL59, and CL60, compared to site CL57. For sites CL56, CL59, and CL60, distinct peaks in the net sulfate reduction rate were observed at the depth of the SMTZs. This indicates that most of the sulfate was consumed within the SMTZ, which confirms that SD-AOM is a key process at these sites (**Figure 5**). In contrast, a relatively lower net sulfate reduction rate was observed at the SMTZ at site CL57. This indicates that most of the downwards diffusing sulfate was reduced by the oxidation of organic matter in the sediment. while sulfate consumption fueled by upwards diffusing methane is insignificant supported by very low net SRR at the SMTZ. It was demonstrated that the SALP pattern during sulfate reduction is relatively unaffected during sulfate diffusion or advection (Antler et al., 2013; Fotherby et al., 2021). Thus, it can be inferred that the differences in the SALP patterns (below ~200 cmbsf) between site CL57 and the three other sites reflect a variation of the dominant sulfate reduction mode (i.e., OSR vs. SD-AOM). The higher SALP value from site CL57 indicates a lower net SRR during OSR and very

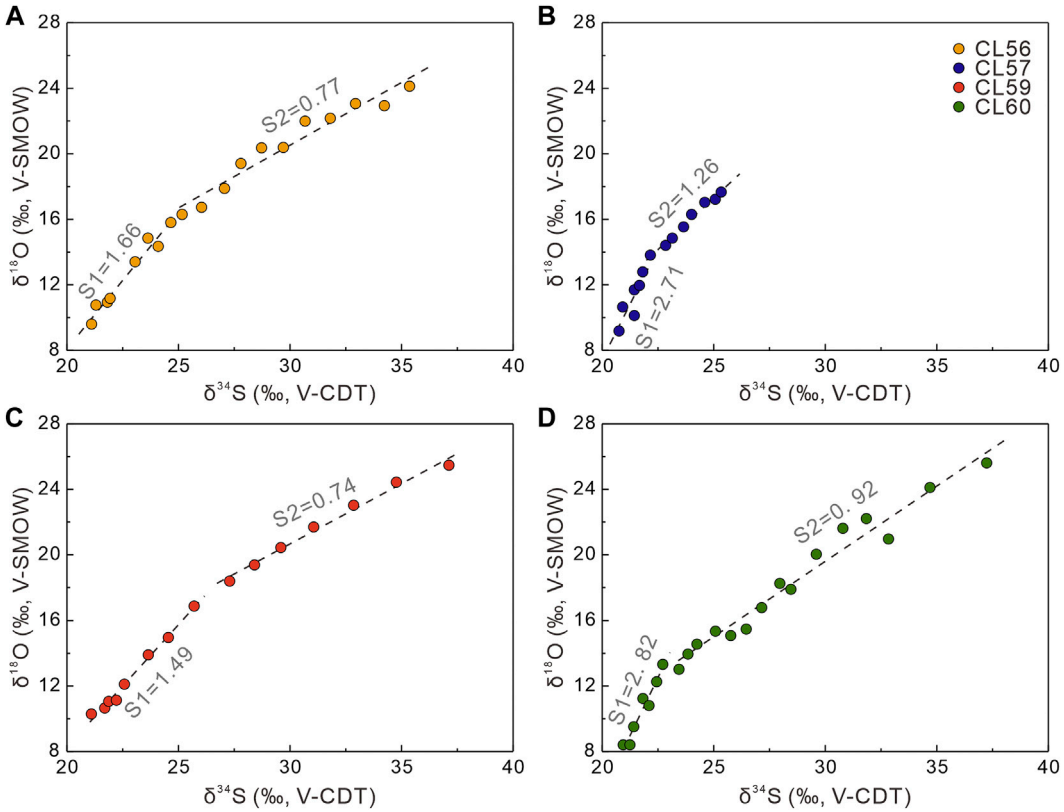

FIGURE 8 | Plots of $\delta^{18}O_{SO4}$ versus $\delta^{34}S_{SO4}$ of **(A)** CL56, **(B)** CL57, **(C)** CL59, and **(D)** CL60. The linear fittings (dash lines) indicate the slope of the apparent linear phase of the $\delta^{18}O_{SO4}$ versus $\delta^{34}S_{SO4}$ cross-plots (SALP), where S1 represents the SALP of shallow part at ~ 200 cmbsf and S2 represents the SALP of deeper part below ~200 cmbsf.

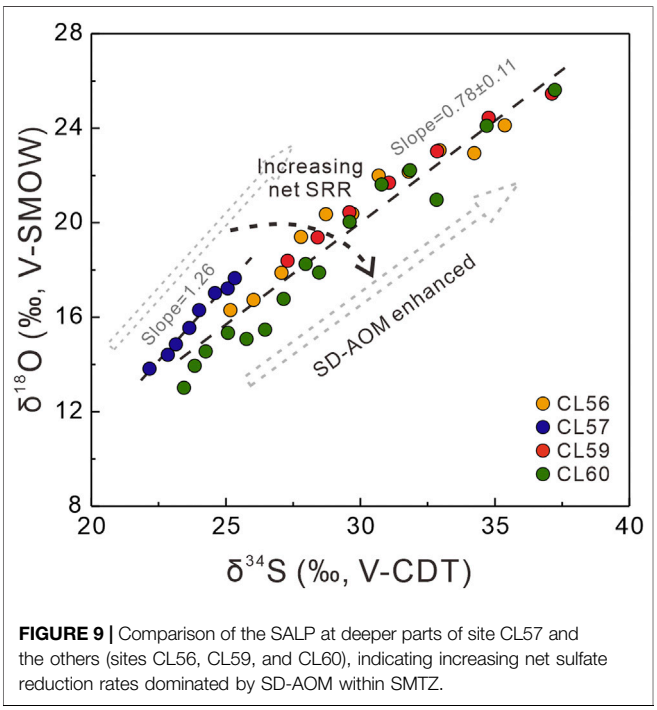

FIGURE 9 | Comparison of the SALP at deeper parts of site CL57 and the others (sites CL56, CL59, and CL60), indicating increasing net sulfate reduction rates dominated by SD-AOM within SMTZ.

limited SD-AOM at this location. In contrast, the lower SALP values for sites CL56, CL59, and CL60 likely reflect more intense SD-AOM at the SMTZs, due to a higher net SRR, although a contribution from OSR cannot be excluded.

CONCLUSION

In this study, pore water and bulk sediment geochemistry was analyzed to decipher how organoclastic sulfate reduction (OSR) and sulfate-driven anaerobic oxidation of methane (SD-AOM) affect the sulfur and oxygen isotopic compositions of dissolved sulfate in methane diffusing environments. Sulfate and DIC profiles as well as the calculated net sulfate reduction rates suggest that OSR is dominant at site CL57, and OSR and SD-AOM likely co-occurred at sites CL56, CL59, and CL60. The patterns of $\delta^{18}O_{SO4}$ versus $\delta^{34}S_{SO4}$ for all study sites are similar to those derived from methane-limited environments. However, different slopes in $\delta^{18}O_{SO4}$ versus $\delta^{34}S_{SO4}$ cross-plot were recognized for site CL57 (a slope of 1.26) and for the other three sites (slopes of 0.78 ± 0.11). It was inferred that the slopes in $\delta^{18}O_{SO4}$ versus $\delta^{34}S_{SO4}$ cross-plot for the study sites are mainly controlled by the dominant sulfate reduction process (i.e., OSR and SD-AOM). Results from this study further improves our

understanding for applying a cross-plot of $\delta^{18}O_{SO4}$ versus $\delta^{34}S_{SO4}$ value as a proxy for identifying the dominant mode of sulfate reduction in modern and ancient marine sediments.

DATA AVAILABILITY STATEMENT

The original contributions presented in the study are included in the article/**Supplementary Material**, further inquiries can be directed to the corresponding authors.

AUTHOR CONTRIBUTIONS

TC, XS, and ZL conceived this study; XS and ZL supervise the investigation; TC and ZL wrote the draft of the manuscript; HS revised the manuscript JL, YL, XY, HL, ZW, and XL performed the mineral selection and analysis of those samples.

FUNDING

This research was jointly funded and supported by the National Key Research and Development Program of China (2018YFC0310004), the Natural Science Foundation of China (No. 41806049, 41876038, and 91128101), the Fundamental Research Funds for the Central Universities (No. 18lgpy28), China Postdoctoral Science Foundation (No. 2018M631015), the Guangdong Special Fund for Economic Development (Marine Economy, No. GDME-2018D001), and the China Geological Survey Project for South China Sea Gas Hydrate Resource Exploration (No. DD20160211).

ACKNOWLEDGMENTS

ZL further acknowledges the International Postdoctoral Exchange Fellowship Program provided by China Postdoctoral Council (No. 20180053). A. Fugmann are thanked for his skillful assistance in the stable isotope lab in Münster.

SUPPLEMENTARY MATERIAL

The Supplementary Material for this article can be found online at: https://www.frontiersin.org/articles/10.3389/feart.2022.862333/full#supplementary-material

REFERENCES

Aharon, P., and Fu, B. (2000). Microbial Sulfate Reduction Rates and Sulfur and Oxygen Isotope Fractionations at Oil and Gas Seeps in deepwater Gulf of Mexico. *Geochimica et Cosmochimica Acta* 64, 233–246. doi:10.1016/S0016-7037(99)00292-6

Aharon, P., and Fu, B. (2003). Sulfur and Oxygen Isotopes of Coeval Sulfate-Sulfide in Pore Fluids of Cold Seep Sediments with Sharp Redox Gradients. *Chem. Geology.* 195, 201–218. doi:10.1016/S0009-2541(02)00395-9

Aller, R. C., Madrid, V., Chistoserdov, A., Aller, J. Y., and Heilbrun, C. (2010). Unsteady Diagenetic Processes and Sulfur Biogeochemistry in Tropical Deltaic Muds: Implications for Oceanic Isotope Cycles and the Sedimentary Record. *Geochimica et Cosmochimica Acta* 74, 4671–4692. doi:10.1016/j.gca.2010.05.008

Antler, G., and Pellerin, A. (2018). A Critical Look at the Combined Use of Sulfur and Oxygen Isotopes to Study Microbial Metabolisms in Methane-Rich Environments. *Front. Microbiol.* 9, 519. doi:10.3389/fmicb.2018.00519

Antler, G., Turchyn, A. V., Herut, B., Davies, A., Rennie, V. C. F., and Sivan, O. (2014). Sulfur and Oxygen Isotope Tracing of Sulfate Driven Anaerobic Methane Oxidation in Estuarine Sediments. *Estuarine, Coastal Shelf Sci.* 142, 4–11. doi:10.1016/j.ecss.2014.03.001

Antler, G., Turchyn, A. V., Herut, B., and Sivan, O. (2015). A Unique Isotopic Fingerprint of Sulfate-Driven Anaerobic Oxidation of Methane. *Geology* 43, 619–622. doi:10.1130/G36688.1

Antler, G., Turchyn, A. V., Rennie, V., Herut, B., and Sivan, O. (2013). Coupled Sulfur and Oxygen Isotope Insight into Bacterial Sulfate Reduction in the Natural Environment. *Geochimica et Cosmochimica Acta* 118, 98–117. doi:10.1016/j.gca.2013.05.005

Berg, P., Risgaard-Petersen, N., and Rysgaard, S. (1998). Interpretation of Measured Concentration Profiles in Sediment Pore Water. *Limnol. Oceanogr.* 43, 1500–1510. doi:10.4319/lo.1998.43.7.1500

Berner, R. A. (1980). *Early Diagenesis: A Theoretical Approach*. Princeton, New Jersey: Princeton University Press, 241.

Blake, R. E., Surkov, A. V., Böttcher, M. E., Ferdelman, T. G., Jørgensen, B. B., and Ferdelman, M. (2006). Oxygen Isotope Composition of Dissolved Sulfate in Deep-Sea Sediments: Eastern Equatorial Pacific Ocean. *Proc. Ocean Drill. Progr. Sci. Results* 201, 1–24. doi:10.2973/odp.proc.sr.201.116.2006

Boetius, A., Ravenschlag, K., Schubert, C. J., Rickert, D., Widdel, F., Gieseke, A., et al. (2000). A marine Microbial Consortium Apparently Mediating Anaerobic Oxidation of Methane. *Nature* 407, 623–626. doi:10.1038/35036572

Borowski, W. S., Hoehler, T. M., Alperin, M. J., Rodriguez, N. M., and Paull, C. K. (2000). Significance of Anaerobic Methane Oxidation in Methane-Rich Sediments Overlying the Blake Ridge Gas Hydrates. *Proc. Ocean Drill. Progr. Sci. Results* 164, 87–99. doi:10.2973/odp.proc.sr.164.214.2000

Borowski, W. S., Paull, C. K., and Ussler, W. (1999). Global and Local Variations of Interstitial Sulfate Gradients in Deep-Water, continental Margin Sediments: Sensitivity to Underlying Methane and Gas Hydrates. *Mar. Geology.* 159, 131–154. doi:10.1016/S0025-3227(99)00004-3

Borowski, W. S., Paull, C. K., and Ussler, W. (1996). Marine Pore-Water Sulfate Profiles Indicate *In Situ* Methane Flux from Underlying Gas Hydrate. *Geol* 24, 655–658. doi:10.1130/0091-7613(1996)024<0655:mpwspi>2.3.co;2

Böttcher, M. E., Bernasconi, S. M., and Brumsack, H.-J. (1999). Carbon, Sulfur, and Oxygen Isotope Geochemistry of Interstitial Waters from the Western Mediterranean. *Proc. Ocean Drill. Progr. Sci. Results* 161, 413–421. doi:10.2973/odp.proc.sr.161.229.1999

Böttcher, M. E., Brumsack, H.-J., and De Lange, G. J. (1998). Sulfate Reduction and Related Stable Isotope (34S, 18O) Variations in Interstitial Waters from the Eastern Mediterranean. *Proc. Ocean Drill. Progr. Sci. Results* 160, 365–376. doi:10.2973/odp.proc.sr.160.002.1998

Böttcher, M. E., Ferdelman, T. G., Jørgensen, B. B., Blake, R. E., Surkov, A. V., and Claypool, G. E. (2006). Sulfur Isotope Fractionation by the Deep Biosphere within Sediments of the Eastern Equatorial Pacific and Peru Margin. *Proc. Ocean Drill. Progr. Sci. Results* 201, 1–21. doi:10.2973/odp.proc.sr.201.109.2006

Böttcher, M. E., and Thamdrup, B. (2001). Anaerobic Sulfide Oxidation and Stable Isotope Fractionation Associated with Bacterial Sulfur Disproportionation in the Presence of MnO_2. *Geochim. Cosmochim. Acta* 65, 1573–1581. doi:10.1016/S0016-7037(00)00622-0

Brunner, B., and Bernasconi, S. M. (2005). A Revised Isotope Fractionation Model for Dissimilatory Sulfate Reduction in Sulfate Reducing Bacteria. *Geochimica et Cosmochimica Acta* 69, 4759–4771. doi:10.1016/j.gca.2005.04.015

Brunner, B., Bernasconi, S. M., Kleikemper, J., and Schroth, M. H. (2005). A Model for Oxygen and Sulfur Isotope Fractionation in Sulfate during Bacterial Sulfate Reduction Processes. *Geochimica et Cosmochimica Acta* 69, 4773–4785. doi:10.1016/j.gca.2005.04.017

Brunner, B., Einsiedl, F., Arnold, G. L., Müller, I., Templer, S., and Bernasconi, S. M. (2012). The Reversibility of Dissimilatory Sulphate Reduction and the Cell-Internal Multi-step Reduction of Sulphite to Sulphide: Insights from the Oxygen Isotope Composition of Sulphate. *Isotopes Environ. Health Stud.* 48, 33–54. doi:10.1080/10256016.2011.608128

Canfield, D. E., Kristensen, E., and Thamdrup, B. (2005). Aquatic Geomicrobiology. *Adv. Mar. Biol.* 48, 1–599. doi:10.1016/00253227(93)90147-n10.1016/S0065-2881(05)48017-7

Canfield, D. E. (2001). 12. Biogeochemistry of Sulfur Isotopes. *Rev. Mineral. Geochem.* 43, 607–636. doi:10.2138/gsrmg.43.1.60710.1515/9781501508745-015

Canfield, D. E., Olesen, C. A., and Cox, R. P. (2006). Temperature and its Control of Isotope Fractionation by a Sulfate-Reducing Bacterium. *Geochimica et Cosmochimica Acta* 70, 548–561. doi:10.1016/j.gca.2005.10.028

Canfield, D. E., Raiswell, R., Westrich, J. T., Reaves, C. M., and Berner, R. A. (1986). The Use of Chromium Reduction in the Analysis of Reduced Inorganic Sulfur in Sediments and Shales. *Chem. Geology.* 54, 149–155. doi:10.1016/00092541(86)90078-110.1016/0009-2541(86)90078-1

Chatterjee, S., Dickens, G. R., Bhatnagar, G., Chapman, W. G., Dugan, B., Snyder, G. T., et al. (2011). Pore Water Sulfate, Alkalinity, and Carbon Isotope Profiles in Shallow Sediment above marine Gas Hydrate Systems: A Numerical Modeling Perspective. *J. Geophys. Res.* 116, B09103. doi:10.1029/2011JB008290

Chen, Y., Ussler, W., Haflidason, H., Lepland, A., Rise, L., Hovland, M., et al. (2010). Sources of Methane Inferred from Pore-Water δ13C of Dissolved Inorganic Carbon in Pockmark G11, Offshore Mid-Norway. *Chem. Geology.* 275, 127–138. doi:10.1016/j.chemgeo.2010.04.013

Claypool, G., Milkov, A. V., Lee, Y.-J., Torres, M. E., Borowski, W. S., and Tomaru, H. (2006). Microbial Methane Generation and Gas Transport in Shallow Sediments of an Accretionary Complex, Southern Hydrate Ridge (ODP Leg 204), Offshore Oregon, USA. *Proc. Ocean Drill. Progr. Sci. Results* 204, 1–52. doi:10.2973/odp.proc.sr10.2973/odp.proc.sr.204.113.2006

Coffin, R., Hamdan, L., Hamdan, L., Plummer, R., Smith, J., Gardner, J., et al. (2008). Analysis of Methane and Sulfate Flux in Methane-Charged Sediments from the Mississippi Canyon, Gulf of Mexico. *Mar. Pet. Geology.* 25, 977–987. doi:10.1016/j.marpetgeo.2008.01.014

Dickens, G. R. (2001). Sulfate Profiles and Barium Fronts in Sediment on the Blake Ridge: Present and Past Methane Fluxes through a Large Gas Hydrate Reservoir. *Geochimica et Cosmochimica Acta* 65, 529–543. doi:10.1016/S0016-7037(00)00556-1

Eckert, T., Brunner, B., Edwards, E. A., and Wortmann, U. G. (2011). Microbially Mediated Re-oxidation of Sulfide during Dissimilatory Sulfate Reduction by Desulfobacter Latus. *Geochimica et Cosmochimica Acta* 75, 3469–3485. doi:10.1016/j.gca.2011.03.034

Egger, M., Riedinger, N., Mogollón, J. M., and Jørgensen, B. B. (2018). Global Diffusive Fluxes of Methane in marine Sediments. *Nat. Geosci* 11, 421–425. doi:10.1038/s41561-018-0122-8

Farquhar, J., Canfield, D. E., Masterson, A., Bao, H., and Johnston, D. (2008). Sulfur and Oxygen Isotope Study of Sulfate Reduction in Experiments with Natural Populations from Fællestrand, Denmark. *Geochimica et Cosmochimica Acta* 72, 2805–2821. doi:10.1016/j.gca.2008.03.013

Feng, D., and Chen, D. (2015). Authigenic Carbonates from an Active Cold Seep of the Northern South China Sea: New Insights into Fluid Sources and Past Seepage Activity. *Deep Sea Res. Part Topical Stud. Oceanography* 122, 74–83. doi:10.1016/j.dsr2.2015.02.003

Feng, D., Peng, Y., Bao, H., Peckmann, J., Roberts, H. H., and Chen, D. (2016). A Carbonate-Based Proxy for Sulfate-Driven Anaerobic Oxidation of Methane. *Geology* 44, 999–1002. doi:10.1130/G38233.1

Fossing, H., Ferdelman, T. G., and Berg, P. (2000). Sulfate Reduction and Methane Oxidation in continental Margin Sediments Influenced by Irrigation (South-East Atlantic off Namibia). *Geochimica et Cosmochimica Acta* 64, 897–910. doi:10.1016/S00167037(99)00349-X10.1016/s0016-7037(99)00349-x

Fotherby, A., Bradbury, H. J., Antler, G., Sun, X., Druhan, J. L., and Turchyn, A. V. (2021). Modelling the Effects of Non-steady State Transport Dynamics on the Sulfur and Oxygen Isotope Composition of Sulfate in Sedimentary Pore Fluids. *Front. Earth Sci.* 8, 587085. doi:10.3389/feart.2020.587085

Fritz, P., Basharmal, G. M., Drimmie, R. J., Ibsen, J., and Qureshi, R. M. (1989). Oxygen Isotope Exchange between Sulphate and Water during Bacterial Reduction of Sulphate. *Chem. Geology. Isotope Geosci. section* 79, 99–105. doi:10.1016/0168-9622(89)90012-2

Froelich, P. N., Klinkhammer, G. P., Bender, M. L., Luedtke, N. A., Heath, G. R., Cullen, D., et al. (1979). Early Oxidation of Organic Matter in Pelagic Sediments of the Eastern Equatorial Atlantic: Suboxic Diagenesis. *Geochimica et Cosmochimica Acta* 43, 1075–1090. doi:10.1016/0016-7037(79)90095-4

Gong, S., Feng, D., Peng, Y., Peckmann, J., Wang, X., Hu, Y., et al. (2021). Deciphering the Sulfur and Oxygen Isotope Patterns of Sulfate-Driven Anaerobic Oxidation of Methane. *Chem. Geology.* 581, 120394. doi:10.1016/j.chemgeo.2021.120394

Han, X., Suess, E., Huang, Y., Wu, N., Bohrmann, G., Su, X., et al. (2008). Jiulong Methane Reef: Microbial Mediation of Seep Carbonates in the South China Sea. *Mar. Geology.* 249, 243–256. doi:10.1016/j.margeo.2007.11.012

Hensen, C., Zabel, M., Pfeifer, K., Schwenk, T., Kasten, S., Riedinger, N., et al. (2003). Control of Sulfate Pore-Water Profiles by Sedimentary Events and the Significance of Anaerobic Oxidation of Methane for the Burial of Sulfur in marine Sediments. *Geochimica et Cosmochimica Acta* 67, 2631–2647. doi:10.1016/S0016-7037(03)00199-6

Hinrichs, K.-U., Hayes, J. M., Sylva, S. P., Brewer, P. G., and DeLong, E. F. (1999). Methane-consuming Archaebacteria in marine Sediments. *Nature* 398, 802–805. doi:10.1038/19751

Hoehler, T. M., Borowski, W. S., Alperin, M. J., Rodriguez, N. M., and Paull, C. K. (2000). Model, Stable Isotope, and Radiotracer Characterization of Anaerobic Methane Oxidation in Gas Hydrate-Bearing Sediments of the Blake Ridge. *Proc. Ocean Drill. Progr. Sci. Results* 164, 79–85. doi:10.2973/odp.proc.sr.164.242.2000

Hu, Y., Feng, D., Liang, Q., Xia, Z., Chen, L., and Chen, D. (2015). Impact of Anaerobic Oxidation of Methane on the Geochemical Cycle of Redox-Sensitive Elements at Cold-Seep Sites of the Northern South China Sea. *Deep Sea Res. Part Topical Stud. Oceanography* 122, 84–94. doi:10.1016/j.dsr2.2015.06.012

Hu, Y., Feng, D., Peckmann, J., Gong, S., Liang, Q., Wang, H., et al. (2020). The Impact of Diffusive Transport of Methane on Pore-Water and Sediment Geochemistry Constrained by Authigenic Enrichments of Carbon, Sulfur, and Trace Elements: A Case Study from the Shenhu Area of the South China Sea. *Chem. Geology.* 553, 119805. doi:10.1016/j.chemgeo.2020.119805

Iversen, N., and Jørgensen, B. B. (1993). Diffusion Coefficients of Sulfate and Methane in marine Sediments: Influence of Porosity. *Geochimica et Cosmochimica Acta* 57, 571–578. doi:10.1016/0016-7037(93)90368-7

Jiang, S.-Y., Yang, T., Ge, L., Yang, J.-H., Ling, H.-F., Wu, N.-Y., et al. (2008). Geochemistry of Pore Waters from the Xisha Trough, Northern South China Sea and Their Implications for Gas Hydrates. *J. Oceanogr.* 64, 459–470. doi:10.1007/s10872-008-0039-8

Johnston, D. T., Gill, B. C., Masterson, A., Gill, B. C., Masterson, A., Beirne, E., et al. (2014). Placing an Upper Limit on Cryptic marine sulphur Cycling. *Nature* 513, 530–533. doi:10.1038/nature13698

Jørgensen, B. B., Findlay, A. J., and Pellerin, A. (2019). The Biogeochemical Sulfur Cycle of Marine Sediments. *Front. Microbiol.* 10, 849. doi:10.3389/fmicb.2019.00849

Jørgensen, B. B., and Kasten, S. (2006). "Sulfur Cycling and Methane Oxidation," in *Marine Geochemistry*. Editors H. D. Schulz and M. Zabel (Berlin-Heidelberg: Springer), 271–309. doi:10.1007/3-540-32144-6_8

Jørgensen, B. B. (1982). Mineralization of Organic Matter in the Sea Bed-The Role of Sulphate Reduction. *Nature* 296, 643–645. doi:10.1038/296643a0

Kastner, M., Claypool, G., and Robertson, G. (2008). Geochemical Constraints on the Origin of the Pore Fluids and Gas Hydrate Distribution at Atwater Valley and Keathley Canyon, Northern Gulf of Mexico. *Mar. Pet. Geology.* 25, 860–872. doi:10.1016/j.marpetgeo.2008.01.022

Komada, T., Burdige, D. J., Li, H.-L., Magen, C., Chanton, J. P., and Cada, A. K. (2016). Organic Matter Cycling across the Sulfate-Methane Transition Zone of the Santa Barbara Basin, California Borderland. *Geochimica et Cosmochimica Acta* 176, 259–278. doi:10.1016/j.gca.2015.12.022

Li, G., Moridis, G. J., Zhang, K., and Li, X.-S. (2010). Evaluation of Gas Production Potential from marine Gas Hydrate Deposits in Shenhu Area of South China Sea. *Energy Fuels* 24, 6018–6033. doi:10.1021/ef100930m

Liang, Q., Hu, Y., Feng, D., Peckmann, J., Chen, L., Yang, S., et al. (2017). Authigenic Carbonates from Newly Discovered Active Cold Seeps on the Northwestern Slope of the South China Sea: Constraints on Fluid Sources,

Formation Environments, and Seepage Dynamics. *Deep Sea Res. Oceanographic Res. Pap.* 124, 31–41. doi:10.1016/j.dsr.2017.04.015

Lin, Z., Sun, X., Peckmann, J., Lu, Y., Xu, L., Strauss, H., et al. (2016). How Sulfate-Driven Anaerobic Oxidation of Methane Affects the Sulfur Isotopic Composition of Pyrite: A SIMS Study from the South China Sea. *Chem. Geology.* 440, 26–41. doi:10.1016/j.chemgeo.2016.07.007

Lin, Z., Sun, X., Strauss, H., Lu, Y., Böttcher, M. E., Teichert, B. M. A., et al. (2018). Multiple Sulfur Isotopic Evidence for the Origin of Elemental Sulfur in an Iron-Dominated Gas Hydrate-Bearing Sedimentary Environment. *Mar. Geology.* 403, 271–284. doi:10.1016/j.margeo.2018.06.010

Lin, Z., Sun, X., Strauss, H., Lu, Y., Gong, J., Xu, L., et al. (2017). Multiple Sulfur Isotope Constraints on Sulfate-Driven Anaerobic Oxidation of Methane: Evidence from Authigenic Pyrite in Seepage Areas of the South China Sea. *Geochimica et Cosmochimica Acta* 211, 153–173. doi:10.1016/j.gca.2017.05.015

Liu, W., Wu, Z., Xu, S., Wei, J., Peng, X., Li, J., et al. (2020). Pore-water Dissolved Inorganic Carbon Sources and Cycling in the Shallow Sediments of the Haima Cold Seeps, South China Sea. *J. Asian Earth Sci.* 201, 104495. doi:10.1016/j.jseaes.2020.104495

Liu, X., Zhang, M., Li, A., Fan, D., Dong, J., Jiao, C., et al. (2021). Depositional Control on Carbon and Sulfur Preservation Onshore and Offshore the Oujiang Estuary: Implications for the C/S Ratio as a Salinity Indicator. *Continental Shelf Res.* 227, 104510. doi:10.1016/j.csr.2021.104510

Luff, R., and Wallmann, K. (2003). Fluid Flow, Methane Fluxes, Carbonate Precipitation and Biogeochemical Turnover in Gas Hydrate-Bearing Sediments at Hydrate Ridge, Cascadia Margin: Numerical Modeling and Mass Balances. *Geochimica et Cosmochimica Acta* 67, 3403–3421. doi:10.1016/S0016-7037(03)00127-3

Luo, M., Chen, L., Wang, S., Yan, W., Wang, H., and Chen, D. (2013). Pockmark Activity Inferred from Pore Water Geochemistry in Shallow Sediments of the Pockmark Field in Southwestern Xisha Uplift, Northwestern South China Sea. *Mar. Pet. Geology.* 48, 247–259. doi:10.1016/j.marpetgeo.2013.08.018

Malinverno, A., and Pohlman, J. W. (2011). Modeling Sulfate Reduction in Methane Hydrate-Bearing continental Margin Sediments: Does a Sulfate-Methane Transition Require Anaerobic Oxidation of Methane? *Geochem. Geophys. Geosyst.* 12, a–n. doi:10.1029/2011GC003501

Martens, C. S., and Berner, R. A. (1974). Methane Production in the Interstitial Waters of Sulfate-Depleted marine Sediments. *Science* 185, 1167–1169. doi:10.1126/science.185.4157.1167

Masuzawa, T., Handa, N., Kitagawa, H., and Kusakabe, M. (1992). Sulfate Reduction Using Methane in Sediments beneath a Bathyal "Cold Seep" Giant Clam Community off Hatsushima Island, Sagami Bay, Japan. *Earth Planet. Sci. Lett.* 110, 39–50. doi:10.1016/0012-821X(92)90037-V

Miao, X., Feng, X., Liu, X., Li, J., and Wei, J. (2021). Effects of Methane Seepage Activity on the Morphology and Geochemistry of Authigenic Pyrite. *Mar. Pet. Geology.* 133, 105231. doi:10.1016/j.marpetgeo.2021.105231

Minami, H., Tatsumi, K., Hachikubo, A., Yamashita, S., Sakagami, H., Takahashi, N., et al. (2012). Possible Variation in Methane Flux Caused by Gas Hydrate Formation on the Northeastern continental Slope off Sakhalin Island, Russia. *Geo-mar. Lett.* 32, 525–534. doi:10.1007/s00367-012-0287-x

Mizutani, Y., and Rafter, T. A. (1973). Isotopic Behaviour of Sulphate Oxygen in the Bacterial Reduction of Sulphate. *Geochem. J.* 6, 183–191. doi:10.2343/geochemj.6.183

Niewöhner, C., Hensen, C., Kasten, S., Zabel, M., and Schulz, H. D. (1998). Deep Sulfate Reduction Completely Mediated by Anaerobic Methane Oxidation in Sediments of the Upwelling Area off Namibia. *Geochim. Cosmochim. Acta* 62, 455–464. doi:10.1016/S0016-7037(98)00055-6

Orphan, V. J., House, C. H., Hinrichs, K.-U., Mckeegan, K. D., and Delong, E. F. (2001). Methane-consuming Archaea Revealed by Directly Coupled Isotopic and Phylogenetic Analysis. *Science* 293, 484–487. doi:10.1126/science.1061338

Reeburgh, W. S. (1980). Anaerobic Methane Oxidation: Rate Depth Distributions in Skan Bay Sediments. *Earth Planet. Sci. Lett.* 47, 345–352. doi:10.1016/0012-821X(80)90021-7

Reeburgh, W. S. (2014). "Global Methane Biogeochemistry," in *Treatise on Geochemistry*. Editors H. D. Holland and K. K. Turekian. Second Edition (Oxford: Elsevier), 71–94. doi:10.1016/B978-0-08-095975-7.00403-4

Reeburgh, W. S. (2007). Oceanic Methane Biogeochemistry. *Chem. Rev.* 107, 486–513. doi:10.1021/cr050362v

Rees, C. E. (1973). A Steady-State Model for sulphur Isotope Fractionation in Bacterial Reduction Processes. *Geochimica et Cosmochimica Acta* 37, 1141–1162. doi:10.1016/0016-7037(73)90052-5

Regnier, P., Dale, A. W., Arndt, S., LaRowe, D. E., Mogollón, J., and Van Cappellen, P. (2011). Quantitative Analysis of Anaerobic Oxidation of Methane (AOM) in marine Sediments: A Modeling Perspective. *Earth-Science Rev.* 106, 105–130. doi:10.1016/j.earscirev.2011.01.002

Rice, C. A., Tuttle, M. L., and Reynolds, R. L. (1993). The Analysis of Forms of Sulfur in Ancient Sediments and Sedimentary Rocks: Comments and Cautions. *Chem. Geology.* 107, 83–95. doi:10.1016/0009-2541(93)90103-P

Rodriguez, N. M., Paull, C. K., and Borowski, W. S. (2000). Zonation of Authigenic Carbonates within Gas Hydrate-Bearing Sedimentary Sections on the Blake Ridge: Offshore Southeastern North America. *Proc. Ocean Drill. Progr. Sci. Results* 164, 301–312. doi:10.2973/odp.proc.sr.164.227.2000

Schulz, H. D. (2006). "Quantification of Early Diagenesis: Dissolved Constituents in Pore Water and Signals in the Solid Phase," in *Marine Geochemistry*. Editors H. D. Schulz and M. Zabel (Berlin-Heidelberg: Springer), 73–124. doi:10.1007/3.540.32144.6_3

Seeberg-Elverfeldt, J., Schlüter, M., Feseker, T., and Kölling, M. (2005). Rhizon Sampling of Porewaters Near the Sediment-Water Interface of Aquatic Systems. *Limnol. Oceanogr. Methods* 3, 361–371. doi:10.4319/lom.2005.3.361

Sivan, O., Schrag, D. P., and Murray, R. W. (2007). Rates of Methanogenesis and Methanotrophy in Deep-Sea Sediments. *Geobiology* 5, 141–151. doi:10.1111/j.1472-4669.2007.00098.x

Strauss, H., Bast, R., Cording, A., Diekrup, D., Fugmann, A., Garbe-Schönberg, D., et al. (2012). Sulphur Diagenesis in the Sediments of the Kiel Bight, SW Baltic Sea, as Reflected by Multiple Stable sulphur Isotopes. *Isotopes Environ. Health Stud.* 48, 166–179. doi:10.1080/10256016.2012.648930

Suess, E. (2005). *RV SONNE Cruise Report SO 177, Sino-German Cooperative Project, South China Sea Continental Margin: Geological Methane Budget and Environmental Effects of Methane Emissions and Gas Hydrates*. IFM-GEOMAR Reports.

Sun, Q., Wu, S., Cartwright, J., and Dong, D. (2012). Shallow Gas and Focused Fluid Flow Systems in the Pearl River Mouth Basin, Northern South China Sea. *Mar. Geology.* 315-318, 1–14. doi:10.1016/j.margeo.2012.05.003

Tong, H., Feng, D., Cheng, H., Yang, S., Wang, H., Min, A. G., et al. (2013). Authigenic Carbonates from Seeps on the Northern continental Slope of the South China Sea: New Insights into Fluid Sources and Geochronology. *Mar. Pet. Geology.* 43, 260–271. doi:10.1016/j.marpetgeo.2013.01.011

Tostevin, R., Turchyn, A. V., Farquhar, J., Johnston, D. T., Eldridge, D. L., Bishop, J. K. B., et al. (2014). Multiple Sulfur Isotope Constraints on the Modern Sulfur Cycle. *Earth Planet. Sci. Lett.* 396, 14–21. doi:10.1016/j.epsl.2014.03.057

Treude, T., Niggemann, J., Kallmeyer, J., Wintersteller, P., Schubert, C. J., Boetius, A., et al. (2005). Anaerobic Oxidation of Methane and Sulfate Reduction along the Chilean continental Margin. *Geochimica et Cosmochimica Acta* 69, 2767–2779. doi:10.1016/j.gca.2005.01.002

Turchyn, A. V., Antler, G., Byrne, D., Miller, M., and Hodell, D. A. (2016). Microbial Sulfur Metabolism Evidenced from Pore Fluid Isotope Geochemistry at Site U1385. *Glob. Planet. Change* 141, 82–90. doi:10.1016/j.gloplacha.2016.03.004

Turchyn, A. V., Brüchert, V., Lyons, T. W., Engel, G. S., Balci, N., Schrag, D. P., et al. (2010). Kinetic Oxygen Isotope Effects during Dissimilatory Sulfate Reduction: A Combined Theoretical and Experimental Approach. *Geochimica et Cosmochimica Acta* 74, 2011–2024. doi:10.1016/j.gca.2010.01.004

Ussler, W., and Paull, C. K. (2008). Rates of Anaerobic Oxidation of Methane and Authigenic Carbonate Mineralization in Methane-Rich Deep-Sea Sediments Inferred from Models and Geochemical Profiles. *Earth Planet. Sci. Lett.* 266, 271–287. doi:10.1016/j.epsl.2007.10.056

Vairavamurthy, M. A., Orr, W. L., and Manowitz, B. (1995). "Geochemical Transformations of Sedimentary Sulfur: an Introduction,". Editors M. A. Vairavamurthy and M. A. A. Schoonen (Washington, D.C: ACS Symposium), 612, 1–14. doi:10.1021/bk-1995-0612.ch001*Geochemical Transformations Sediment. Sulfur*

Valentine, D. L., Blanton, D. C., Reeburgh, W. S., and Kastner, M. (2001). Water Column Methane Oxidation Adjacent to an Area of Active Hydrate Dissociation, Eel River Basin. *Geochimica et Cosmochimica Acta* 65, 2633–2640. doi:10.1016/S0016-7037(01)00625-1

Van Cappellen, P., and Wang, Y. (1996). Cycling of Iron and Manganese in Surface Sediments; a General Theory for the Coupled Transport and Reaction of Carbon, Oxygen, Nitrogen, Sulfur, Iron, and Manganese. *Am. J. Sci.* 296, 197–243. doi:10.2475/ajs.296.3.197

Wallmann, K., Drews, M., Aloisi, G., and Bohrmann, G. (2006). Methane Discharge into the Black Sea and the Global Ocean via Fluid Flow through Submarine Mud Volcanoes. *Earth Planet. Sci. Lett.* 248, 545–560. doi:10.1016/j.epsl.2006.06.026

Wang, X., Collett, T. S., Lee, M. W., Yang, S., Guo, Y., and Wu, S. (2014). Geological Controls on the Occurrence of Gas Hydrate from Core, Downhole Log, and Seismic Data in the Shenhu Area, South China Sea. *Mar. Geology.* 357, 272–292. doi:10.1016/j.margeo.2014.09.040

Wei, J., Liang, J., Lu, J., Zhang, W., and He, Y. (2019). Characteristics and Dynamics of Gas Hydrate Systems in the Northwestern South China Sea - Results of the Fifth Gas Hydrate Drilling Expedition. *Mar. Pet. Geology.* 110, 287–298. doi:10.1016/j.marpetgeo.2019.07.028

Whiticar, M. J., Faber, E., and Schoell, M. (1986). Biogenic Methane Formation in marine and Freshwater Environments: CO2 Reduction vs. Acetate Fermentation-Isotope Evidence. *Geochimica et Cosmochimica Acta* 50, 693–709. doi:10.1016/0016-7037(86)90346-7

Wing, B. A., and Halevy, I. (2014). Intracellular Metabolite Levels Shape Sulfur Isotope Fractionation during Microbial Sulfate Respiration. *Proc. Natl. Acad. Sci. U.S.A.* 111, 18116–18125. doi:10.1073/pnas.1407502111

Wortmann, U. G., Bernasconi, S. M., and Böttcher, M. E. (2001). Hypersulfidic Deep Biosphere Indicates Extreme Sulfur Isotope Fractionation during Single-step Microbial Sulfate Reduction. *Geol* 29, 647–650. doi:10.1130/0091-7613(2001)029<0647:hdbies>2.0.co;2

Wortmann, U. G., Chernyavsky, B., Bernasconi, S. M., Brunner, B., Böttcher, M. E., and Swart, P. K. (2007). Oxygen Isotope Biogeochemistry of Pore Water Sulfate in the Deep Biosphere: Dominance of Isotope Exchange Reactions with Ambient Water during Microbial Sulfate Reduction (ODP Site 1130). *Geochimica et Cosmochimica Acta* 71, 4221–4232. doi:10.1016/j.gca.2007.06.033

Wu, D. D., Wu, N. Y., Zhang, M., Guan, H. X., Fu, S. Y., and Yang, R. (2013a). Relationship of Sulfate-Methane Interface (SMI), Methane Flux and the Underlying Gas Hydrate in Dongsha area,Northern South China Sea. *Earth Sci. J. China Univ. Geosci.* 38, 1309–1320. (in Chinese with English abstract). doi:10.3799/dqkx.2013.128

Wu, D., Wu, N., Ye, Y., Zhang, M., Liu, L., Guan, H., et al. (2011a). Early Diagenesis Records and Pore Water Composition of Methane-Seep Sediments from the Southeast Hainan Basin, South China Sea. *J. Geol. Res.* 2011, 1–10. doi:10.1155/2011/592703

Wu, L., Yang, S., Liang, J., Su, X., Fu, S., Sha, Z., et al. (2013b). Variations of Pore Water Sulfate Gradients in Sediments as Indicator for Underlying Gas Hydrate in Shenhu Area, the South China Sea. *Sci. China Earth Sci.* 56, 530–540. doi:10.1007/s11430-012-4545-6

Wu, N. Y., Yang, S. X., Wang, H. B., Liang, J. Q., Gong, Y. H., Lu, Z. Q., et al. (2009). Gas-bearing Fluid Influx Sub-system for Gas Hydrate Geological System in Shenhu Area, Northern South China Sea. *Chin. J. Geophys.* 52, 1641–1650. (in Chinese with English abstract). doi:10.3969/j.issn.0001-5733.2009.06.027

Wu, N., Zhang, H., Yang, S., Zhang, G., Liang, J., Lu, J. a., et al. (2011b). Gas Hydrate System of Shenhu Area, Northern South China Sea: Geochemical Results. *J. Geol. Res.* 2011, 1–10. doi:10.1155/2011/370298

Yang, S. X., Liang, J. Q., Lu, J. A., Qu, C. W., and Liu, B. (2017). New Understandings on the Characteristics and Controlling Factors of Gas Hydrate Reservoirs in the Shenhu Area on the Northern Slope of the South China Sea. *Earth Sci. Front.* 24, 1–14. doi:10.13745/j.esf.yx.2016-12-43

Yang, T., Jiang, S.-Y., Yang, J.-H., Lu, G., Wu, N.-Y., Liu, J., et al. (2008). Dissolved Inorganic Carbon (DIC) and its Carbon Isotopic Composition in Sediment Pore Waters from the Shenhu Area, Northern South China Sea. *J. Oceanogr.* 64, 303–310. doi:10.1007/s10872-008-0024-2

Yang, T., Jiang, S., Ge, L., Yang, J., Wu, N., Zhang, G., et al. (2010). Geochemical Characteristics of Pore Water in Shallow Sediments from Shenhu Area of South China Sea and Their Significance for Gas Hydrate Occurrence. *Chin. Sci. Bull.* 55, 752–760. doi:10.1007/s11434-009-0312-2

Ye, H., Yang, T., Zhu, G., Jiang, S., and Wu, L. (2016). Pore Water Geochemistry in Shallow Sediments from the Northeastern continental Slope of the South China Sea. *Mar. Pet. Geology.* 75, 68–82. doi:10.1016/j.marpetgeo.2016.03.010

Ye, J., Wei, J., Liang, J., Lu, J., Lu, H., Zhang, W., et al. (2019). Complex Gas Hydrate System in a Gas Chimney, South China Sea. *Mar. Pet. Geology.* 104, 29–39. doi:10.1016/j.marpetgeo.2019.03.023

Yoshinaga, M. Y., Holler, T., Goldhammer, T., Wegener, G., Pohlman, J. W., Brunner, B., et al. (2014). Carbon Isotope Equilibration during Sulphate-Limited Anaerobic Oxidation of Methane. *Nat. Geosci* 7, 190–194. doi:10.1038/NGEO2069

Yu, X., Wang, J., Liang, J., Li, S., Zeng, X., and Li, W. (2014). Depositional Characteristics and Accumulation Model of Gas Hydrates in Northern South China Sea. *Mar. Pet. Geology.* 56, 74–86. doi:10.1016/j.marpetgeo.2014.03.011

Zhang, H. Q., Yang, S. X., Wu, N. Y., Su, X., Holland, M., Schultheiss, P., et al. (2007a). "Successful and Surprising Results for China's First Gas Hydrate Drilling Expedition," in *Fire in the Ice*. National Energy Technology Laboratory, US Department of Energy. (Fall issue 1).

Zhang, H. T., Zhang, H. Q., and Zhu, Y. H. (2007b). Gas Hydrate Investigation and Research in China: Present Status and Progress. *Geol. China* 34, 953–961. (in Chinese with English abstract).

Zhang, W., Liang, J., Wei, J., Su, P., Lin, L., and Huang, W. (2019). Origin of Natural Gases and Associated Gas Hydrates in the Shenhu Area, Northern South China Sea: Results from the China Gas Hydrate Drilling Expeditions. *J. Asian Earth Sci.* 183, 103953. doi:10.1016/J.Jseaes.2019.103953

Conflict of Interest: The authors declare that the research was conducted in the absence of any commercial or financial relationships that could be construed as a potential conflict of interest.

Publisher's Note: All claims expressed in this article are solely those of the authors and do not necessarily represent those of their affiliated organizations, or those of the publisher, the editors and the reviewers. Any product that may be evaluated in this article, or claim that may be made by its manufacturer, is not guaranteed or endorsed by the publisher.